NASA Technical Memorandum 105798

P-56

Flutter Analysis of Supersonic Axial Flow Cascades Using a High Resolution Euler Solver

Part 1: Formulation and Validation

T.S.R. Reddy and Milind A. Bakhle
University of Toledo
Toledo, Ohio

Dennis L. Huff
Lewis Research Center
Cleveland, Ohio

and

Timothy W. Swafford
Mississippi State University
Mississippi State, Mississippi

August 1992

Date for general release August 1994

Flutter Analysis of Supersonic Axial Flow Cascades Using a High Resolution Euler Solver
Part 1: Formulation and Validation

T. S. R. Reddy [*], **Milind A. Bakhle** [**]
University of Toledo, Toledo, Ohio 43606

Dennis L. Huff [†]
NASA Lewis Research Center
Cleveland, Ohio 44135

Timothy W. Swafford [+]
Mississippi State University
Mississippi State, MS

ABSTRACT

This report presents, in two parts, a dynamic aeroelastic stability (flutter) analysis of a cascade of blades in supersonic axial flow. Each blade of the cascade is modeled as a typical section having pitching and plunging degrees of freedom. Aerodynamic forces are obtained from a time accurate, unsteady, two-dimensional cascade solver based on the Euler equations. The solver uses a time marching flux-difference splitting (FDS) scheme. Flutter stability is analyzed in the frequency domain. The unsteady force coefficients required in the analysis are obtained by harmonically oscillating (HO) the blades for a given flow condition, oscillation frequency, and interblade phase angle. The calculated time history of the forces is then Fourier decomposed to give the required unsteady force coefficients. An influence coefficient (IC) method and a pulse response (PR) method are also implemented to reduce the computational time for the calculation of the unsteady force coefficients for any phase angle and oscillation frequency. Part 1, this report, presents these analysis methods, and their validation by comparison with results obtained from linear theory for a selected flat plate cascade geometry. A typical calculation for a rotor airfoil is also included to show the applicability of the present solver for airfoil configurations. The predicted unsteady aerodynamic forces for a selected flat plate cascade geometry, and flow conditions correlated well with those obtained from linear theory for different interblade phase angles and oscillation frequencies. All the three methods of predicting unsteady force coefficients, namely, HO, IC and PR showed good correlation with each other. It was established that only a single calculation with *four* blade passages is required to calculate the aerodynamic forces for *any* phase angle for a cascade consisting of *any* number of blades, for *any* value of the oscillation frequency. Flutter results, including mistuning effects, for a cascade of stator airfoils are presented in Part 2 of the report.

---

[*] Senior Research Associate, Department of Mechanical Engineering

[**] Research Associate, Department of Mechanical Engineering

[†] Research Engineer

[+] Associate Professor, Department of Aerospace Engineering

NOMENCLATURE

a	sonic velocity
$[A]$	matrix of frequency domain aerodynamic coefficients
$\bar{A}$	Roe matrix
b	airfoil semi-chord
c	airfoil chord
c_l	lift coefficient
c_m	moment coefficient about elastic axis
C_p	pressure coefficient $= 2\,(p - p_\infty)\,/\,\rho_\infty V_\infty^2$
$\overline{C_p}$	steady pressure coefficient
ΔC_p	unsteady pressure difference coefficient $= (p_{lower} - p_{upper})\,/\,\rho_\infty V_\infty^2 \times$ amplitude
$\{F\}$	blade aerodynamic load vector
F	flux vector in ξ direction
G	flux vector in η direction
h	plunging displacement, normal to airfoil chord
i	imaginary unit, $\sqrt{-1}$; also index in ξ direction
i	incidence angle
$[I]$	identity matrix
I_α	moment of inertia about elastic axis
Im{ }	imaginary part of { }
j	index in η direction
k_b	reduced frequency, $k_b = \omega b\,/M_\infty a_\infty$
$[K]$	blade stiffness matrix
K_h	spring constant for plunging
K_α	spring constant for pitching
$l_{hh}\,, l_{\alpha h}\,, l_{h\alpha}\,, l_{\alpha\alpha}$	frequency domain unsteady aerodynamic coefficients, Eq. (14)
m	mass of typical section
M	Mach number
$[M]$	blade mass matrix
n	blade index
N	number of blades in the cascade
NB	minimum number of blocks / grids required in computations
N_{k_b}	number of reduced frequencies used in the analysis
N_σ	number of interblade phase angles used in the analysis
q	vector of dependent variables
Q	transformed vector of dependent variables
Q_h	lift
Q_α	moment about elastic axis
r	index for interblade phase angle, Eq. (12a)
r_α	radius of gyration about elastic axis in semi-chord units
Re{ }	real part of { }
s	cascade spacing or gap
s/c	gap-to-chord ratio
S_α	static unbalance

t	time
T_2	total computational time required for two blocks calculations
t/c	thickness-to-chord ratio
x, y	Cartesian coordinates
x_α	distance between elastic axis and center of mass in semi-chord units, see Fig. 1
$\{X\}$	blade displacement vector
V^*	reduced velocity, $V^* = M_\infty a_\infty / b\omega_\alpha$

α	pitching displacement about elastic axis
δ	difference operator
θ	stagger angle
μ	mass ratio
ρ	fluid density
ξ	transformed coordinate
η	transformed coordinate
σ	interblade phase angle
τ	computational time, $\tau = a_\infty t \;/ 2b$
$\Delta\tau$	time step
ω	oscillation frequency
ω_h	uncoupled natural frequency for bending (plunging)
ω_α	uncoupled natural frequency for torsion (pitching)

subscripts and *superscripts*

L, R	left, right of interface
T	transpose of matrix
o	amplitude of harmonic motion
∞	evaluated at far upstream conditions
n	evaluated at time level n
$\ddot{(\,)}$	$d^2(\,)/dt^2$

INTRODUCTION

NASA Lewis Research Center has initiated an exploratory program to investigate the feasibility of a supersonic through flow (SSTF) fan (Refs. 1-3). The SSTF fan is expected to provide about a 10 percent decrease in specific fuel consumption, and about a 25 percent reduction in propulsion system weight, which would lead to a 22 percent increase in aircraft range (Ref. 1). Other advantages of the SSTF fan include fewer fan stages required for a given pressure ratio, less inlet cowl and boundary layer bleed drag, better inlet pressure recovery, and better matching of bypass ratio variation to flight speed. For a safe design of the SSTF fan, analysis is required to check that dynamic aeroelastic instability or flutter will not occurr in the operating range. This report presents a flutter analysis for the SSTF fan blade. Only a two-dimensional (2D) unsteady aerodynamic / aeroelastic analysis has been developed and used, because of the complexity involved in modelling a three-dimensional (3D) rotor / stator in supersonic through flow.

In the 2D unsteady aerodynamic / aeroelastic analysis, the rotor / stator is modelled as a rectilinear two-dimensional cascade of airfoils with supersonic axial flow (Refs. 4-8); this is also referred to as a cascade with a supersonic leading edge locus. Earlier researchers have used linearized equations (see for example Ref. 4) applicable for unloaded cascades of flat plate airfoils in inviscid flow. The motion of the airfoils in each mode of the cascade is assumed to be simple harmonic with a constant phase angle between the adjacent blades. This assumption leads to an eigenvalue problem in the frequency domain and the stability of the system is determined from the eigenvalues (Ref. 9).

The above analyses neglect the effects of airfoil thickness, camber, and steady state angle of attack on supersonic cascade flutter. Recently, an approximate analysis, which includes these effects, was presented in Ref. 10. However, the Mach wave reflection pattern was assumed to be the same as that for a flat plate cascade. This means that the effect of the airfoil profile on the Mach wave pattern and its effect on stability is neglected. One way to rigorously include the effects of airfoil shape (thickness and camber), and steady state angle of attack in cascade flutter analysis is by using Computational Fluid Dynamics (CFD) methods. Recent advances in the field of CFD with regard to the development of more efficient algorithms and increases in computer speed and memory have made numerical studies to compute the complex flow field associated with a supersonic axial flow cascades possible.

Steady aerodynamic characteristics of supersonic compressor airfoils using the Euler/Navier-Stokes equations have been reported in Ref. 11. Recently, results from two-dimensional CFD solvers for the analysis of oscillating cascades in supersonic axial flow have been reported in Refs. 12 and 13. The formulation in Ref. 12 is based on the full-potential equation, and that in Ref. 13 is based on the Euler equations. The discretized form of these equations are solved by the Newton-iteration method for the full potential equation and by an the alternating direction implicit (ADI) method for the Euler equations. The unsteady motion resulting from blade oscillation is included by generating a new grid for every time step in Ref. 12, and by using a deforming grid technique in Ref. 13. These codes have been extended to include aeroelastic analysis both in the time and frequency domains in Refs. 14 and 15.

The present study seeks to improve on the work in Ref. 13 in two respects: (a) the solver of Ref. 13 requires explicit input of artificial viscosity factors to control the numerical stability of the solution, (b) a C-grid has to be used with this version of the ADI solver, which inhibits the true representation of a zero-thickness flat plate airfoil geometry. In order to avoid these difficulties, an Euler solver based on flux difference splitting (FDS) has been developed in Ref. 16. This solver does not require explicit input of artificial dissipation factors, and uses an H-grid which allows for a true representation of flat plate airfoils. This solver was modified to investigate aeroelastic stability of cascades in subsonic flow in Ref. 17.

The objectives of the present study are (1) to extend the capability of the aeroelastic Euler cascade code of Ref. 17 to predict the unsteady aerodynamic forces of a cascade of airfoils in supersonic axial flow, (2) to implement influence coefficient and pulse response methods (Ref. 18) and verify these for supersonic axial flow cascades by comparison with other methods, and (3) to use the forces obtained by the above methods for flutter calculations of selected supersonic axial flow cascades.

This study is restricted to a two-dimensional cascade model. A typical section representation of each of the blades of the cascade is assumed. Two-degrees-of-freedom, plunging and pitching, motion is considered for the analysis. A frequency domain analysis is used to predict flutter. The study is presented in two parts. In part I, this report, the formulation of various methods mentioned in the objectives above are presented and validated by comparing with linear theory results, Ref. 8. Typical flutter calculations, for a tuned rotor, are also presented for both a cascade of flat plates and actual SSTF rotor fan airfoils in supersonic axial flow. Extensive flutter calculations for a cascade of stator airfoils, including mistuning effects, are presented in part II.

FORMULATION

The aeroelastic model and the aerodynamic model are described in this section.

Aeroelastic model

The aeroelastic model for the cascade consists of a typical section with two degrees of freedom (bending and torsion) for each blade; see Fig. 1. Structural damping is not considered at present, although it could be easily included. The equations of motion for each blade of the cascade have the form:

$$m\ddot{h} + S_\alpha \ddot{\alpha} + K_h h = Q_h \tag{1a}$$

$$S_\alpha \ddot{h} + I_\alpha \ddot{\alpha} + K_\alpha \alpha = Q_\alpha \tag{1b}$$

where h is the plunging (bending) displacement, α is the pitching (torsion) displacement, m is the airfoil mass, I_α is the moment of inertia, S_α is the static unbalance, K_h and K_α are the spring constants for plunging and pitching, respectively; Q_h and Q_α are the aerodynamic loads (lift and moment, respectively) and the dots over the various terms indicate differentiation with respect to time. The above equations can be written in matrix notation as

$$[M]\{\ddot{X}\} + [K]\{X\} = \{F\} \tag{2}$$

where

$$[M] = \begin{bmatrix} 1 & x_\alpha \\ x_\alpha & r_\alpha^2 \end{bmatrix} \qquad [K] = \begin{bmatrix} \omega_h^2 & 0 \\ 0 & r_\alpha^2\,\omega_\alpha^2 \end{bmatrix}$$

$$\{X\} = \begin{Bmatrix} h/b \\ \alpha \end{Bmatrix} \qquad \{F\} = \begin{Bmatrix} Q_h/mb \\ Q_\alpha/mb^2 \end{Bmatrix} \tag{3}$$

and $\omega_h = (K_h/m)^{1/2}$ is the uncoupled natural frequency for bending; $\omega_\alpha = (K_\alpha/I_\alpha)^{1/2}$ is the uncoupled natural frequency for torsion; $x_\alpha = S_\alpha/mb$ is the distance between the elastic axis and center of mass in semi-chord units; $r_\alpha = (I_\alpha/mb^2)^{1/2}$ is the radius of gyration about the elastic axis in semi-chord units; and b is the airfoil semi-chord. The aerodynamic loads, Q_h and Q_α, are obtained using the aerodynamic model described below.

Aerodynamic model

The aerodynamic model is based on the unsteady, two-dimensional, Euler equations. The equations in conservative differential form are transformed from a Cartesian reference frame (x,y) to a time dependent body-fitted curvilinear reference frame (ξ,η). This transformation process and the ensuing numerical method are presented in detail in Ref. 19. Hence the following discussion merely highlights the development of the methodology and the reader is encouraged to consult Ref. 19 for more details.

The transformed Euler equations can be written in vector form as

$$\frac{\partial Q}{\partial \tau} + \frac{\partial F}{\partial \xi} + \frac{\partial G}{\partial \eta} = 0 \tag{4}$$

where

$$Q = Jq \tag{5a}$$
$$F = J(\xi_t q + \xi_x f + \xi_y g) \tag{5b}$$
$$G = J(\eta_t q + \eta_x f + \eta_y g) \tag{5c}$$

and

$$q = [\rho, \rho u, \rho v, e]^T \tag{5d}$$
$$f = [\rho u, \rho u^2 + p, \rho u v, u(e+p)]^T \tag{5e}$$
$$g = [\rho v, \rho u v, \rho v^2 + p, v(e+p)]^T \tag{5f}$$

ξ_t , ξ_x , ξ_y , η_t , η_x , and η_y are the metrics, ρ is the fluid density, u and v are the velocities in Cartesian frame, e is the energy, p is the fluid pressure and J is the Jacobian of transformation.

The approach taken in the present effort is based on the integration of these equations over a discrete set of contiguous cells (volumes) in computational space and is generally referred to as a finite volume method. This discretization results in the following expression where cell centers are denoted as i, j:

$$\frac{\partial Q}{\partial \tau} + \frac{\delta_i F}{\Delta \xi} + \frac{\delta_j G}{\Delta \eta} = 0 \qquad \text{(6a)}$$

With $\Delta\xi = \Delta\eta = 1$ (by definition), this becomes

$$\frac{\partial Q}{\partial \tau} = -(\delta_i F + \delta_j G) \qquad \text{(6b)}$$

where

$$\delta_i() = ()_{i+1/2} - ()_{i-1/2} \quad \text{and} \quad \delta_j() = ()_{j+1/2} - ()_{j-1/2}$$

A consequence of the finite volume formulation is that components of the dependent vector Q within a particular cell represent average values over that cell. However, it is evident from the above representation of flux differences that a method is needed to allow these fluxes to be accurately represented at cell faces. As discussed in Ref. 19, the method used in the present effort is based on the one-dimensional Riemann solver of Roe (Ref. 20) at cell interfaces for each coordinate direction. The method uses as a basis the following approximate equation which represents a quasilinear form of a locally one-dimensional conservation law:

$$\frac{\partial q}{\partial t} + \overline{A}(q_L, q_R)\frac{\partial q}{\partial x} = 0 \qquad \text{(7)}$$

where q is the untransformed dependent variable vector, and $\overline{A}(q_L, q_R)$ is a constant matrix representative of local cell interface conditions which is constructed using so-called "Roe-averaged" variables. The determination of the eigensystem of $\overline{A}$ and knowing that the change in dependent variables across an interface is proportional to the right eigenvectors allows first order flux formulas to be constructed. This approach to extracting flowfield information from characteristically dictated directions is commonly referred to as flux difference splitting (FDS) and is applicable to multidimensional space if the assumption is made that all wave propagation occurs normal to a particular cell interface. To provide higher order spatial accuracy, a corrective flux is appended to the first order flux discussed above. In addition, in order to control dispersive errors commonly encountered with higher order schemes, so-called limiters are used to limit components of the interface flux resulting in total variation diminishing (TVD) schemes. All solutions presented herein were obtained using third order spatial accuracy in conjunction with the minmod limiter (Ref. 19).

An implicit scheme is used to integrate Eq. (5) in time and can be written as a general class of schemes (Ref. 21):

$$\left[I + \frac{\Theta \Delta \tau}{1+\psi} M^n \right] \Delta Q^n = - \left(\frac{\Delta \tau}{1+\psi} \right) R^n + \left(\frac{\psi}{1+\psi} \right) \Delta Q^{n-1} \tag{8}$$

A three point backward ($\Theta = 1$, $\psi = 1/2$) method is used in the present work which results in second order temporal accuracy. As discussed in Ref. 19, all terms appearing in the above equation should be comprised of elements which result from one flux formula. However, experience has shown that computations performed using FDS theory on the right hand side of the above equation (i.e. in the residual term) and flux vector split (FVS) theory (Ref. 22) on the left hand side are superior to those obtained using FDS theory on both right and left sides.

For the present case,

$$M^n = \delta_i A^+ + \delta_i A^- + \delta_j B^+ + \delta_j B^- \tag{9}$$

where

$$A^+ = \left(\frac{\partial F^+}{\partial Q} \right)^n \qquad A^- = \left(\frac{\partial F^-}{\partial Q} \right)^n$$

$$B^+ = \left(\frac{\partial G^+}{\partial Q} \right)^n \qquad B^- = \left(\frac{\partial G^-}{\partial Q} \right)^n$$

F^+, F^-, G^+ and G^- are obtained using FVS theory and the residual given by

$$R^n = \delta_i F^n + \delta_j G^n \tag{10}$$

is obtained by evaluating F and G using FDS theory.

Because of the difficulty and cost of inverting the left hand side of Eq. (8), approximate factorization is used; detailed expressions can be found in Ref. 19.

Grid

The flow equations are solved on one or more passage-centered H-grids. Within a typical grid block (Fig. 2a), the lower computational boundary contains the upper surface of one blade in the cascade, while the upper computational boundary contains the lower surface of the adjacent blade. Periodic boundaries in the blade-to-blade direction extend upstream and downstream from the blade surfaces. The inlet boundary corresponds to the left computational boundary and the outflow corresponds to the right boundary. An algebraic grid generation scheme is used to generate a grid for a single blade passage. This grid is then stacked to form a cascade for multiple blades, see Fig. 2b.

The solver can simulate both pitching and plunging motions, either individually or in combination. The computational grid is deformed such that the airfoils follow a prescribed motion and the grid near the center of the passage remains fixed. This is done using weighting functions. For a given blade passage, the upper and lower boundaries containing the airfoil surfaces move according to an input function (which may be predetermined or calculated from the displacements obtained using a structural model). The grid for that passage is divided into seven sub-regions, as shown in Fig. 2c. The user can fix any portion of the grid near the center of the passage (region VII), where the grid is not affected by the airfoil displacement. The grid smoothly deforms for each time step in the regions between the fixed portion of the grid and the two blade surfaces (regions I to VI). The deforming portion of the grid uses a combination of weighting functions based on spatial and index magnitudes. For each i-index in the deforming computational plane ($1< i <ni$), a weighting function, wj, is calculated to control the amount of deformation in the j-direction:

$$wj_{i,j} = \left| \frac{s_{i,j}}{s_{i,jend}} - 1 \right| \tag{11a}$$

$$s_{i,j} = \sum_{m=jbeg}^{j} \sqrt{(x_{i,m} - x_{i,m-1})^2 + (y_{i,m} - y_{i,m-1})^2} \tag{11b}$$

The values for $jbeg$ and $jend$ in Eqs. (11) depend on the region being deformed. Regions I through III use $jbeg = 1$ and $jend = jfix1$. Likewise, regions IV through VI use $jbeg = nj$ and $jend = jfix2$ (Fig. 2c). In the i-direction, similar weighting functions are used to keep the inlet and exit boundaries fixed:

$$wi_{i,j} = \frac{i-1}{ile-1} \qquad 1 \le i \le ile - 1 \tag{11c}$$

$$wi_{i,j} = 1 \qquad ile \le i \le ite \tag{11d}$$

$$wi_{i,j} = \left| \frac{i - ite - 1}{ni - ite - 1} - 1 \right| \qquad ite + 1 \le i \le ni \tag{11e}$$

Before the grid is deformed, the coordinate system is translated to the desired center of pitching (xtr, ytr):

$$X_{i,j} = x_{i,j} - xtr_{i,j} \tag{11f}$$

$$Y_{i,j} = y_{i,j} - ytr_{i,j} \tag{11g}$$

The pitching and plunging motions of the blades are defined using the following equations:

$$\bar{x}_{i,j} = X_{i,j} \cos(\Delta\alpha) - Y_{i,j} \sin(\Delta\alpha) \tag{11h}$$

$$\bar{y}_{i,j} = Y_{i,j} \cos(\Delta\alpha) + X_{i,j} \sin(\Delta\alpha) + \Delta h \tag{11i}$$

Here, $\Delta\alpha$ and Δh are the respective pitching and plunging displacements. Finally, the new position of the grid (corresponding to the next time step) is calculated:

$$x_{i,j} = X_{i,j} + wi_{i,j}\, wj_{i,j}\,(\bar{x}_{i,j} - X_{i,j}) + xtr_{i,j} \tag{11j}$$

$$y_{i,j} = Y_{i,j} + wi_{i,j}\, wj_{i,j}\,(\bar{y}_{i,j} - Y_{i,j}) + ytr_{i,j} \tag{11k}$$

Boundary Conditions

The computational grids used in the present study employ multiple blocks. A discussion pertaining to how flowfield conditions are imposed along the boundaries of the computational domain is presented next.

Figure 2a represents a single grid block used for calculations with steady flows and flows with in-phase blade motions. The airfoil upper and lower surfaces are located along lines B-C and F-G, respectively where solid wall boundary conditions are employed. Lines A-E and D-H represent inflow and outflow boundaries, respectively. The inlet conditions are assumed to be uniform by specifying the flow density, velocity, flow angle, and pressure. The exit flow variables are extrapolated from the interior by using simple first-order model. Periodicity is imposed between lines A-B and E-F, and lines C-D and G-H.

For harmonic blade motions with constant phase difference (interblade phase angle) between adjacent blades, N grid blocks (passages) are generally required; N is the number of blades in the cascade. The values of interblade phase angle (σ) that can occur are given, Ref. 23, as

$$\sigma_r = 2\pi r / N \qquad r = 0, 1, 2, \cdots, N-1 \tag{12a}$$

Then, the minimum number of grid blocks, NB, required for a given σ is given as

$$NB = \textit{smallest integer}\ [\,(360/\sigma),\, 360/(360-\sigma),\, N\,] \tag{12b}$$

For example, for $\sigma = 180$ deg, two grid blocks are required. This is shown in Fig. 2d. For this case, periodicity is enforced between lines A-B and I-J, and lines C-D and K-L, respectively. Also lines A-I and D-L become inflow and outflow boundaries, respectively. Continuity of flowfield variables is imposed between adjacent blocks (E-F and G-H) by simple injection (see Fig. 2d with regard to the use of interior and phantom cells of adjacent blocks).

A similar procedure is followed for other interblade phase angles which generally require additional blade passages. However, in supersonic axial flow, the domain of the flow field can be reduced by inspecting the shock structures through the cascade; see Fig. 3. In supersonic axial flow, no disturbance can exist upstream of the leading edges of the blades and the wakes behind the blades cannot influence the flow in the blade passages. The disturbances generated inside the Mach cone of the leading edge do not influence the flow outside the cone, which means that only three blades need to be considered in the solutions. For example, consider the cascade geometry defined in Fig. 3, and let the blades be denoted as shown, the blade '*ref*' being the reference blade; let the flow conditions be defined such that the bow shock off the leading edge intersects the adjacent blade surfaces. The flow above blade '*ref*+1' and below blade '*ref*−1' will have no influence on the surface pressure on blade '*ref*'. For this reason, the boundary conditions on the upper and lower boundaries, A-B,C-D and I-J, K-L in Fig. 2d, of the global grid (the grid containing two blocks) can be *arbitrary*. This means that for harmonic blade motions, *only two blocks* have to be considered in computation for *any* interblade phase angle. However, only the surface pressures on the reference blade are correct for the specified interblade phase angle.

Flutter Analysis

Assuming small amplitude oscillations, Eqs. (2), can be solved for flutter (stability) in frequency domain. The frequency domain approach, which is suitable only for linear problems, is described below for a tuned cascade. In a tuned cascade, all blades are identical and thus have identical values of structural parameters.

The displacements for each blade of the cascade are assumed to be harmonic functions of time:

$$\{X\} = \{X_o\} e^{i(\omega t + n\sigma)} \qquad n = 0, 1, 2, \cdots, N-1 \tag{13}$$

where N is the number of blades in the cascade, n is a blade index and ω is the frequency of oscillation. Further, the aerodynamic loads are assumed to be *linear* functions of the displacements:

$$Q_h = \pi\rho_\infty b^3\omega^2 [\, l_{hh}(h/b) + l_{h\alpha}(\alpha) \,] \tag{14a}$$

$$Q_\alpha = \pi\rho_\infty b^4\omega^2 [\, l_{\alpha h}(h/b) + l_{\alpha\alpha}(\alpha) \,] \tag{14b}$$

or

$$\{F\} = \left(\frac{\omega^2}{\mu}\right) [A]\{X\}$$

where $\mu = m/\pi\rho_\infty b^2$ is the mass ratio and $[A]$ is the matrix of frequency domain unsteady aerodynamic coefficients:

$$[A] = \begin{bmatrix} l_{hh} & l_{h\alpha} \\ l_{\alpha h} & l_{\alpha\alpha} \end{bmatrix}$$

It should be noted that the elements of $[A]$ are functions of the cascade geometry, flow conditions, ω and σ.

The aeroelastic equations yield an eigenvalue problem (for each blade):

$$\left[[K]^{-1}[M] + \frac{1}{\mu}[K]^{-1}[A] \right]\{X\} = \frac{1}{\omega^2}\{X\} \tag{15}$$

For a tuned cascade, the same eigenvalue problem is obtained for each blade, Ref. 9. Hence, it is sufficient to solve this problem for just *one* of the blades (but for each value of σ). The two eigenvalues obtained from the solution are generally complex. The real part of the eigenvalue determines the stability of the system; the system is said to flutter if the real part of either eigenvalue is positive.

The frequency domain aerodynamic coefficients (l_{hh} , $l_{\alpha h}$, etc.) are obtained from the unsteady Euler solver using one of the three methods described below. These methods are valid for small amplitude blade oscillations for which the unsteady flowfield is linearly dependent on the amplitude. A steady flowfield has to be obtained first for the given cascade geometry (stagger angle, θ and gap-to-chord ratio, s/c) and specified inlet conditions (Mach number and incidence angle). Then the aerodynamic coefficients are calculated.

1. *Forced Harmonic Oscillation (HO) method*

Starting with the steady flowfield, the airfoil motions are specified as sinusoidal variations in time with a fixed interblade phase angle between adjacent blades:

plunging: $$h = h_0 \sin(2k_b M_\infty \tau + n\sigma) \tag{16}$$

pitching: $$\alpha = \alpha_0 \sin(2k_b M_\infty \tau + n\sigma) \tag{17}$$

$$n = 0, 1, 2, \cdots , NB-1$$

where $k_b = \omega b / M_\infty a_\infty$ is the reduced frequency based on airfoil semi-chord and $\tau = a_\infty t / 2b$ is a non-dimensional time.

The Euler equations are marched in time, with the motion as specified above. After the initial transients have decayed, the lift and moment coefficients show a periodic variation with time. The variation of the lift and moment coefficients is recorded as a function of time. This time history is then decomposed into Fourier components to obtain the complex frequency-domain aerodynamic coefficients. This procedure must be done separately for each blade motion – plunging and pitching. It must then be repeated for each possible value of interblade phase angle. For a cascade with N blades, the values of interblade phase angle at which flutter can occur are given by Eq. (12a).

As mentioned earlier, the forced harmonic oscillation method requires only two blocks for computation for any interblade phase angle. This is true irrespective of the number of blades in the cascade. However, the Euler equations have to be solved separately for each possible interblade phase angle, Eq. (12a). A method to obtain the coefficients for all possible interblade phase angles in a single calculation is described below.

2. *Influence Coefficient (IC) Method*

The influence coefficient method, Ref. 18, is based on the principle of linear superposition and it has been verified experimentally in Ref. 24. Briefly, the solution to a linear problem is obtained by superposing the solutions to the individual elemental problems that comprise the original problem. Since the method is based on the principle of linear superposition, it is valid only for linear problems.

The problem to be solved is one of a cascade of N blades in which each blade oscillates with a motion of the form $\sin(\omega t + n\sigma_r)$, where n is the blade index that varies from 0 to $N-1$, and σ_r is the interblade phase angle given by Eq. (12a). This problem is divided into N elemental problems. The k^{th} elemental problem consists of the same cascade of N blades in which all blades, except one, are stationary and the k^{th} blade oscillates with a motion of the form $\sin(\omega t)$. The original problem and all the elemental problems have solutions that are harmonic functions of time.

For the problem in which all blades oscillate with a motion of the form $e^{i(\omega t+n\sigma_r)}$, the forces ($c_l$ and c_m) on the zeroth blade can be represented as $Q_0 e^{i\omega t}$; Q_0 is complex valued to allow the force to lead or lag the motion. Denoting the force on the 0^{th} blade in the k^{th} elemental problem as the influence coefficient $Q_{0,k}$, the force Q_0 for a given σ_r is obtained by superposition

$$Q_0(\sigma_r) = \sum_{k=0}^{N-1} Q_{0,k} e^{ik\sigma_r} \tag{18}$$

Further, due to the spatial periodicity of the cascade, only the relative positions of the oscillating blade and the reference (zeroth) blade are important. That is, the forces generated on the 0^{th} blade due to the oscillation of the k^{th} blade are equal to the forces on the 1^{st} blade due to the oscillation of the $k+1^{th}$ blade, and so on. Thus,

$$Q_{0,k} = Q_{-k,0} = Q_{N-k,0} \tag{19}$$

where the periodicity of the cascade of N blades has been invoked again in the last step. Eq. (18) can be written in terms of influence coefficients as

$$Q_0(\sigma_r) = \sum_{k=1}^{N} Q_{N-k,0} e^{ik\sigma_r} \tag{20a}$$

Replacing the influence coefficients $Q_{0,k}$ by the coefficients $Q_{N-k,0}$ means that all the required influence coefficients can be calculated simultaneously rather than separately. That is, instead of oscillating the k^{th} blade, calculating the force history on the 0^{th} blade and then repeating for all values of k between 0 and $N-1$, it is possible to oscillate the 0^{th} blade and determine the forces on all blades simultaneously. This means that the computational effort required for the calculation of all the influence coefficients can be reduced by a factor of N.

For supersonic axial flow cascades, for which the aerodynamic domain of influence is contained within the adjacent blade passages, there is no influence on the reference blade from blades which are more than one blade (pitch) away. This indicates that it is sufficient to calculate the correct forces on just three blades, namely the reference blade and ones on either side. Therefore, Eq. (20) can be written as

$$Q_{ref}\ (\sigma_r) = Q_{ref,ref} + Q_{ref+1,ref}\ e^{-i\sigma_r} + Q_{ref-1,ref}\ e^{i\sigma_r} \qquad (20b)$$

where the blade indices *ref*, *ref*+1 and *ref*−1 refer to the reference blade, the blade above it and the blade below it, respectively; see Fig. 4. In the present analysis, four blocks are used to calculate the unsteady forces on the three blades. Thus, using the IC method with four blocks in computations, the aerodynamic coefficients can be calculated for *all* interblade phase angles at a given oscillation frequency. This is true irrespective of the number of blades (N) in the cascade. It should be noted that it is possible to calulate the forces on the three blades using two blocks instead of four; this requires some code modifications, not attempted here.

The forced harmonic oscillation method and the influence coefficient method require that the Euler equations have to be solved separately for each oscillation frequency of interest. A method to obtain the coefficients for all frequencies in a single calculation is described below.

3. *Pulse Response (PR) method*

This method has evolved from the indicial approach that is widely used in many different fields. The indicial response is the response, lift or moment, to a step change in the given mode of motion. From the indicial response, the response for any arbitrary motion, specifically harmonic motion, can be calculated using Duhamel's superposition integral.

Let the time-dependence of the blade motion be denoted as $f(t)$ and let the corresponding response be denoted as $F(t)$. Let $F_\delta(t)$ denote the response corresponding to a unit step function, $f(t) = \delta(t)$. The response corresponding to an arbitrary motion $f(t)$ can be written using Duhamel's superposition integral:

$$F(t) = \int_0^t F_\delta(t-\zeta)\ \dot{f}(\zeta)\,d\zeta \qquad (21)$$

Using the above equation, the response to a harmonic motion, $f(t) = e^{i\omega t}$, can be determined:

$$F(t) = \int_0^t F_\delta(t-\zeta)\, i\omega\, e^{i\omega\zeta}\, d\zeta \qquad (22)$$

Since only periodic response is desired, consider the above integral in the limit as $t \to \infty$. Using a change of variable and extending the lower limit to $-\infty$, gives

$$F(t) = i\omega\, \overline{F_\delta}(\omega) e^{i\omega t} \qquad (23)$$

where $\overline{F_\delta}(\omega)$ is the Fourier transform of $F_\delta(t)$ given as

$$\overline{F_\delta}(\omega) = \int_{-\infty}^{+\infty} F_\delta(t)\, e^{-i\omega t}\, dt \tag{24}$$

For an arbitrary motion $f(t)$ and the corresponding response $F(t)$, the Fourier transform of Eq. (21) gives:

$$\overline{F}(\omega) = i\omega\, \overline{F_\delta}(\omega)\, \overline{f}(\omega)$$

or

$$i\omega \overline{F_\delta}(\omega) = \overline{F}(\omega) \,/\, \overline{f}(\omega) \tag{25}$$

where $\overline{f}(\omega)$ and $\overline{F}(\omega)$ are the Fourier transforms of $f(t)$ and $F(t)$, respectively. Eq. (25) indicates that the response to harmonic blade motion can be determined using any arbitrary motion $f(t)$ and the corresponding response $F(t)$.

Over the course of time, to avoid numerical difficulties, the step change in displacement has been replaced by a smooth step function and finally by a pulse. In the pulse motion, the blade returns to its original position after the duration of the pulse. This is in contrast to the step motion in which the blade positions are different before and after the step. The pulse motion thus allows the flowfield to return to its steady undisturbed state after the transients created by the pulse have decayed. The unsteady calculations therefore need to be carried out only long enough to ensure that the solution has reached its final state (the same as the initial state) within some specified tolerance.

Out of the different pulse shapes investigated, Ref. 18 has suggested use of the following pulse which is used in the present calculations:

$$\begin{aligned} f(t) &= 4\left(\frac{t}{t_{max}}\right)^2 \exp\left(2 - \frac{1}{1 - t/t_{max}}\right) && \text{for } 0 \le t < t_{max} \\ f(t) &= 0 && \text{for } t \ge t_{max} \end{aligned} \tag{26}$$

where t_{max} is the duration of the pulse. The above choice makes $f(t)$ and $\dot{f}(t)$ vanish at $t = 0$ and $t = t_{max}$; in addition, higher derivatives also go to zero at $t = t_{max}$. This ensures that there is a smooth transition to and from the undisturbed blade position.

The pulse response method can be used in conjunction with the influence coefficient method to obtain the frequency domain aerodynamic coefficients for each possible interblade phase angle and for specified frequencies of oscillation, as follows. One blade in the cascade is given a transient motion of the form $h(t) = h_o f(t)$ or $\alpha(t) = \alpha_o f(t)$. The calculations start with the steady solution and unsteady response to the pulse in either motion, plunging or pitching, is calculated until the transient flowfield reaches the steady flowfield within a specified tolerance. The motion as well as the response on all the blades (four in this case) are recorded and Fourier transforms of these are calculated numerically for the frequency of interest. Using these transforms, the influence coefficients ($Q_{k,0}$) are calculated from Eq. (25); it is to be noted that the harmonic response, $i\omega \overline{F_{\delta}}(\omega)$, obtained from Eq. (25) for this case, is simply the influence coefficient ($Q_{k,0}$). Eq. (20b) is then used to calculate the frequency domain unsteady aerodynamic coefficients for the interblade phase angle of interest. In this way, the coefficients can be determined for various values of reduced frequency by calculating the Fourier transforms for the frequency of interest using the same time histories.

The computational implementation of the three methods, HO, IC and PR, is shown in Fig. 4. It shows the number of blocks used, and the associated blade motion.

RESULTS

The analysis methods presented in the previous section are applied to investigate the behavior of oscillating cascades in supersonic axial flow. First, unsteady pressure distributions are calculated for a flat plate cascade using the forced harmonic oscillations (HO) method, Eqs. (16) and (17); the results are compared with published results to help validate the Euler solver. Then, the unsteady lift and moment coefficients are compared with those obtained from the influence coefficient (IC) method and the pulse response (PR) method. Next, frequency domain flutter calculations are performed for a flat plate cascade and the results are verified by comparison with results from linear theory. Finally, flutter predictions are presented for a rotor airfoil cascade, oscillating in coupled pitching and plunging motion.

All the calculations are performed for the supersonic axial flow rotor (cascade) geometry given in Ref. 8. The cascade has 58 blades (N=58), a gap-to-chord ratio (s/c) of 0.311 and a stagger angle (θ) of 28.0 deg. The inlet Mach number (M_{∞}) is 2.61. All of the Euler solutions are obtained using a H-grid for each passage. A typical grid is shown in Fig. 2a for the rotor airfoil cascade and in Fig. 5 for the flat plate cascade. A 91×41 (streamwise by pitchwise) grid is used both for flat plate airfoils and rotor airfoils; an algebraic grid generation scheme is used to generate this grid. The inlet boundary is located only 0.3 chordlengths upstream from the leading edge because, in supersonic axial flow, no disturbance can travel upstream from the leading edge of the airfoil. There are 20 points in the streamwise direction in the region between the inlet boundary and the leading edge. There are 50 points along each surface of the airfoil, and 21 points beyond the trailing edge. The time step has been varied to check its effect on convergence and accuracy. The calculations have been performed on a Cray Y-MP computer. The solver takes about 5×10^{-5} CPU seconds per time step per grid point per block.

Code Validation

1. *Results from the forced harmonic method*

A cascade of flat plate airfoils is considered. The incidence angle (i) is 0 deg. The reduced frequency based on semi-chord (k_b) is 0.5 The cascade is oscillated in pitch about the 30% of chord location, with an amplitude of oscillation (α_0) of 0.1 deg. The equations are time marched for a given interblade phase angle, until a periodic solution is obtained. Four cycles of oscillation were found to be sufficient for the solutions to become periodic in time as shown in Fig. 6a. The results from the last cycle are Fourier decomposed to obtain the real and imaginary quantities.

Figs. 6b and 6c show the predicted unsteady pressure distributions (first harmonic pressure difference coefficient, ΔC_p , versus chord) for $\sigma = 0$ and 180 deg, respectively. These interblade phase angles require a minimum of one, and two grid blocks for numerical calculations, respectively. The results from linear theory (Ref. 4) are also plotted for comparison. For flat plate airfoils and small amplitudes of oscillation, the present calculations are expected to agree with the linear theory of Ref. 4. The results for the two interblade phase angles are in good agreement with those of Ref. 4. Note that some smearing of the pressure distribution occurs near the reflected Mach wave locations; however, the computed ΔC_p 's pass through the mid-point of the high and low values of pressure at the discontinuity. Figure 6d shows the Mach contour lines predicted by the present solver. The locations at which the Mach waves strike the airfoil ($x/c = 0.52$ on the upper surface and $x/c = 0.81$ on the upper surface) compare well with the locations given by linear theory.

Results are now presented for the flat plate cascade undergoing plunging motions; these results are compared with results from linear theory. The amplitude of oscillation is, $h_0/c = 3\times10^{-4}$. The time response of lift coefficient is shown in Fig. 7a, indicating that the response has become periodic. Figures 7b and 7c show pressure distribution comparisons for $\sigma = 0$ and 180 deg, respectively. As for the pitching motion cases, the agreement between the Euler predictions and linear theory is good. These comparisons validate the present Euler solver for the two interblade phase angles.

It was mentioned earlier that two blocks are sufficient for calculations at any interblade phase angle in supersonic axial flow. To verify this, calculations are performed using two block, four block, and eight block configurations for ten interblade phase angles. It should be noted here that two blocks represent $\sigma = 0$ and 180 deg exactly; four blocks represent $\sigma = 0$, 90, 180, 270 deg exactly; and eight blocks represent $\sigma = 0$, 45, 90, 135, 180, 225, 270, 315 deg exactly. Figure 8a shows the plot of moment coefficient versus interblade phase angle. The cascade is pitching about 30% chord. It can be seen that all the three configurations give the same value indicating that for the supersonic axial flow solution, two blocks are sufficient to obtain coefficients for any interblade phase angle. Similar comparison for lift coefficient is shown in Fig. 8b. Results for plunging motion, not presented here, show the same trend.

The variation of moment coefficient with interblade phase angle is compared with that obtained from the linear theory of Ref. 4, and from the ADI-Euler analysis of Ref. 13 in Fig. 9a. The cascade is pitching about 30% chord. Excellent agreement is seen with linear theory results. The discrepancy with those of Ref. 13 may be due to the fact that the flat plate airfoil used in the calculations of Ref. 13 was not infinitely thin but had a finite thickness, which resulted in each airfoil having a blunt leading edge affecting the Mach wave structure. Figure 9b shows the lift coefficient versus interblade phase angle for the cascade oscillating in plunge. Again, excellent agreement is seen. As mentioned above, all the calculations are performed using only two blocks in the computation.

Next, the calculated force coefficients for varying reduced frequencies are compared with those obtained from linear theory. Figure 10 shows this comparison for a pitching cascade. Figure 10a shows the lift and Fig. 10b shows the moment coefficients for $\sigma = 0$ deg; Fig. 10c shows the lift and Fig. 10d shows the moment for $\sigma = 180$ deg. The corresponding results for plunging motion are shown in Figs. 11a - 11d. Excellent agreement is seen with the results from linear theory even for reduced frequencies as high as 2.0. It should be noted that although some smearing of pressure distributions occurred near shock locations (Fig. 6b-7c), all the force coefficients showed good agreement with the corresponding results from linear theory.

This completes the validation of the present solver for supersonic axial flow calculations for harmonic motions. It should be noted that for the above cases, for unsteady runs, about 268 steps per cycle were required with four cycles of oscillations. This corresponds to a nondimensional time step of 8.98×10^{-3}. For the amplitudes of oscillation considered, it was found that unsteady flowfield was linearly related to the amplitude of oscillation, Fig. 11e. Therefore, the unsteady aerodynamic pressures can be obtained from the influence coefficient method and pulse response method. The results obtained from these methods are compared with results from the harmonic oscillation method in the following sections.

2. *Results from the influence coefficient method*

As mentioned earlier, four blocks are used in the influence coefficient (IC) method, see Fig. 4b. The cascade parameters are again $s/c = 0.311$, $\theta = 28$ deg, $M_\infty = 2.61$, $i = 0$ deg and $k_b = 0.5$. The reference blade in the cascade is given a forced harmonic motion in pitch about 30% of the chord, Eqs. (16); the remaining blades remain stationary. The amplitude of oscillation used in the calculations is $\alpha_0 = 0.1$ deg. Ten interblade phase angles are considered for calculation and comparison purposes. The time step used is the same as that in previous calculations, and the response on all the blades is calculated. Then, the required coefficients for all the values of σ are obtained using Eq. (20b). The results from forced harmonic oscillation (HO) method are obtained separately for each interblade phase angle, each run taking about one-half hour of CPU time; the total time being about five CPU hours for the required ten interblade phase angles. With the influence coefficient (IC) method, it takes about one CPU hour, a saving factor of five. Figures 12a and 12b show the comparison of the lift and moment coefficients due to pitching motion at various interblade phase angles. The results show that the HO method and the IC method give identical results. It may be recalled that the HO method and the linear theory showed excellent agreement, as noted earlier. This verifies the superposition principle and the associated calculations. It implicitly confirms that the unsteady problem is linear for the amplitude of oscillation considered in the calculations. Figures 13a and 13b show the lift and moment coefficients due to plunging; good agreement is seen between the HO and IC methods.

Since the rotor cascade has 58 blades, the implementation of the HO method requires 58 separate computations (runs) with two blocks to obtain aerodynamic coefficients for all interblade phase angles. With the IC method, only one computation with *four* blocks is required to obtain aerodynamic coefficients for *all* the 58 interblade phase angles. In fact, this is true for any rotor having any number of blades. However, the HO and IC methods have to be repeated for each oscillation frequency; this is avoided by using a combination of the influence coefficient (IC) and pulse response (PR) methods as seen below.

3. *Results from combined pulse response and influence coefficient method*

Next the pulse response (PR) method, combined with the IC method, is used to obtain unsteady aerodynamic coefficients at various frequencies and interblade phase angles. The cascade is oscillated in pitch about 30% chord. The calculations are performed for different pulse durations. For pulse durations of 134, 268 and 402 time steps, identical results were obtained for the frequencies studied. Again, only four blocks are used in the computations. As before, only the reference blade is given the pulse motion (Fig. 4c) and the response on all the blades is calculated. The calculations are continued until all responses have returned to the initial undisturbed values. The time histories are Fourier transformed and combined according to Eq. (25) to obtain the influence coefficients ($Q_{k,0}$) which are combined according to Eq. (20b) to get the harmonic coefficients. Figures 14a and 14b show the comparison of lift and moment for pitching motion about mid-chord for $\sigma = 0$ deg for various reduced frequencies. Excellent agreement can be seen between the predictions from the HO method and the PR+IC method. Figures 14c and 14d show the lift and moment coefficients for $\sigma = 180$ deg; the same agreement is seen. The corresponding results for plunging motion, presented in Figs. 15a - 15d, show the same good agreement. Results for other interblade phase angles, not shown here, showed similar good agreement. This validates the implementation of the PR method in conjunction with the IC method.

As mentioned above, using the IC and PR methods with four blocks, the aerodynamic coefficients for all 58 interblade phase angles, and all reduced frequencies of interest can be obtained, with minimal computational effort. The calculations presented above show the validity of the Euler solver, and the implementation of the HO, IC, and PR methods. These methods are subsequently used in the flutter calculations of the supersonic rotor.

4. *Relative computational costs for HO, IC and PR+IC methods*

The computational time required for the calculation of aerodynamic coefficients using each of the three methods can be estimated as follows. For the sake of conciseness, it is assumed that the total number of time steps in each of the calculations is the same. Let N_σ be the number of interblade phase angles (usually equal to N), and let N_{k_b} be the number of reduced frequencies for which calculations are to be performed. Let T_2 be the computational time for a single calculation using two grid blocks. Table I shows the total computational time for all phase angles and frequencies for each of the calculation methods. Compared to the HO method, the computational time for the IC method is reduced by a factor of $N_\sigma / 2$ and that for the PR+IC method by $N_\sigma N_{k_b} / 2$. As an example, for 58 interblade phase angles and 4 reduced frequencies, the saving factor is 29 using the IC method, and 116 using the PR+IC method.

Supersonic compressor rotor blade

Results are now presented for a cascade of airfoils, corresponding to the rotor of a supersonic compressor. The cascade parameters are the same as for the flat plate cascade. However, the thickness-to-chord ratio of the airfoil is 0.05 and an incidence angle of $i = 8$ deg is used in the calculations. The grid used in the calculations is shown in Fig. 16a.

Steady loading

Figure 16b shows the convergence of the numerical scheme for steady solution. A critical examination of the numerical values showed that the forces converged to fourth decimal place after 2500 steps. Fig. 16c shows the distribution of steady pressure coefficient ($\overline{C_p}$) predicted by the present solver. It is compared with the results obtained from the ADI-Euler solver of Ref. 13. A good qualitative agreement is seen. Fig. 16d shows the steady pressure distribution comparison with that obtained from the code described in Ref. 11, which is based on a solution of the thin layer Navier-Stokes equations. The present solver predicts the shocks to be located about 10% down stream of the position predicted by Ref. 11. The discrepancy is probably because viscous effects and quasi-3D effects are included in the analysis of Ref. 11, whereas the present analysis is a 2D inviscid one.

Unsteady loading

The unsteady pressure distribution is now calculated for the rotor cascade oscillating in pitch and plunge. Time history of the moment coefficient, for pitching motion about the 30% of chord location, is shown in Fig. 17a. The pressure difference coefficient (ΔC_p), real and imaginary, is shown in Fig. 17b for $\sigma = 0$ deg and in Fig. 17c for $\sigma = 180$ deg. Results from linear theory are also shown for comparison. It should be noted that linear theory of Lane (Ref. 4) does not account for airfoil loading (thickness and camber). Accordingly, significant differences are seen between the pressure distributions predicted by the present analysis and linear theory; see Figs. 17b and 17c. From these figures, it can be noted that the locations of the shock are shifted considerably due to the airfoil camber and thickness. The shock from the leading edge impinges at a point 20% upstream of that predicted by linear theory and the reflected shock at a point 20% downstream. Figure 17d shows the Mach contour lines predicted by the present solver. A comparison with Fig. 6d shows the effect of airfoil shape on the reflected Mach wave pattern. Figure 18a shows the time response of lift for plunging motion; the unsteady pressure distribution is shown in Fig. 18b and Fig. 18c. Significant differences are seen between the present results and those from linear theory.

The moment coefficient for pitching about the 30% of chord location is compared in Fig. 19 with that obtained from linear theory. This shows only a slight change in the value of the reduced frequency at which the imaginary moment coefficient becomes zero. This is attributed to the effect of airfoil thickness and angle of attack. It is surprising to note that the integrated force coefficients do not differ much from those predicted by linear theory even though the Mach reflection pattern and the associated unsteady pressure distributions are quite different.

Figures 20a and 20b show the results obtained from the influence coefficient and pulse response methods for the rotor airfoil. The results are compared with those obtained from the forced harmonic oscillation method. The comparisons show that even for airfoils with thickness and camber, the IC and PR methods give good correlation with HO method.

Flutter Calculations

The example considered is a tuned compressor cascade with 58 blades. The geometric and structural parameters correspond to the rotor configuration studied above. The structural model for each blade is a typical section (pitching and plunging). The pitching axis position is at 30% chord. This location was found to be critical for flutter in Ref. 8. The radius of gyration is $r_\alpha = 0.588$ and the elastic axis is located at the center of mass ($x_\alpha = 0$); the ratio of natural frequencies in bending and torsion is $\omega_h/\omega_\alpha = 0.567$; the mass ratio is $\mu = 456$.

The flutter calculations in frequency domain, (for a fixed Mach number) require an inner loop on interblade phase angle, with an outer loop on reduced frequency. Using the HO method, this can be done as follows. Starting with the steady flowfield, a value of reduced frequency (k_b) is selected and the airfoils are forced in plunging motion with a specified interblade phase angle (σ) until the flowfield becomes periodic in time. The lift and moment coefficients are calculated at each time step and stored; these are later decomposed into Fourier components to obtain the frequency domain aerodynamic coefficients. This procedure is repeated for pitching motion. In this way all four frequency domain aerodynamic coefficients corresponding to the specified values of reduced frequency and phase angle are determined. The eigenvalue problem given by Eq. (15) is then solved. The real part of the eigenvalue determines the stability; the system is stable for the selected values of k_b and σ if the real part of both eigenvalues is negative. The preceding steps are repeated for the remaining values of σ. For a cascade with 58 blades, flutter can occur at any of the value of σ given by Eq. (12a). If the cascade is found to be stable at all interblade phase angles, then a lower value of reduced frequency is selected. This is continued until the real part of one of the eigenvalues changes sign; this defines the flutter condition.

With the successful implementation of the PR+IC method the unsteady aerodynamic coefficients for different k_b and all σ can be calculated in a smaller amount of CPU time. Only four blade passages are considered in the calculations. One of the blades is given a pulse, and the responses are recorded as mentioned earlier. Then using the PR+IC method, the coefficients are calculated for each frequency and for each phase angle as shown before, with considerable reduction in CPU time. The flutter stability calculations are verified by performing calculations for a flat plate cascade.

Fig. 21 shows the root locus plot obtained for $k_b = 1.1$. The plot shows the frequency and damping values for 58 interblade phase angles. These values of interblade phase angles, given by Eq. (12a), are 0, 6.2, 12.4, ..., 173.8, 180, 186.2, 192.4, ..., and 353.8 deg; they are indicated in the figure by the arrow starting with σ=0 deg.. Figure 21a shows the first mode, and Fig. 21b shows the second mode. The first mode is stable for all the values of σ. The second mode is unstable for some values of σ. It is interesting to note that the damping values for the first mode are really one order less than for the second mode, even though the first mode damping values are always negative. The figures also show the comparison with the root locus plot obtained from linear theory. Excellent agreement is seen, validating the IC, PR methods, the flutter calculations, and the present Euler aeroelastic solver.

Next, the calculations are repeated for the rotor airfoil cascade for $k_b = 1.1$. The root locus plot is shown in Fig. 22. As before, the first mode (Fig. 22a) is more stable than the second mode (Fig. 22b). However, the following differences between the flat plate and rotor airfoil results are noted. For the first mode (Fig. 22a), the area enclosed by the root locus plot is more for the rotor as compared to the flat plate. The area enveloped is determined by the spread in the frequency and damping due to interblade coupling (cascade effects). Hence, Fig. 22a indicates that there is more cascade effects for the rotor configuration. Further, the values of damping are different for the rotor airfoil and flat plate for the same σ. For the second mode (Fig. 22b), the area enveloped by the root locus plot is nearly the same for both the flat plate and rotor airfoils; however, the orientation of the plot is changed. Also the eigenvalues show an opposite trend in relation to the order of increasing σ. The physical significance of these differences is not clear, except that they are due to the effect of steady loading due to thickness and camber.

For the rotor airfoil cascade, calculations are repeated for different values of reduced frequency until the real part of the eigenvalue changes sign. The phase angle at flutter is $\sigma = 192.4$ deg, the frequency ratio is $\omega / \omega_\alpha = 1.002$ and the reduced frequency is $k_b = 1.09$. The corresponding results for the flat plate cascade are $\sigma = 186.2$ deg, $\omega / \omega_\alpha = 1.002$ and $k_b = 1.153$. This indicates that there is a marginal effect of airfoil shape on stability.

CONCLUSIONS

Aeroelastic stability (flutter) analysis methods using an Euler solver have been presented for supersonic axial flow cascades. The Euler solver is based on a flux difference split algorithm. Results presented have shown the validity of the unsteady Euler solver for harmonic blade oscillations, both in pitching and plunging motions. For harmonic oscillations, where the amplitude of oscillation is within the linear range, influence coefficient and pulse response methods have been developed. These methods have been successfully implemented and are shown to give same values of the aerodynamic coefficients as obtained from harmonic oscillation method. These methods considerably reduced the computational time for obtaining the aerodynamic coefficients required in a frequency domain based flutter analysis. It has been shown that a single calculation using four blade passages is enough to obtain the force coefficients for any interblade phase angle and frequency of interest, irrespective of the number of blades in the cascade.

A two-degrees-of-freedom typical section model has been used for each blade of the cascade for flutter prediction. Each blade in the cascade has pitching and plunging motions. Representative results from a frequency domain flutter analysis have been obtained for a flat plate and for a rotor cascade configuration. Flutter results for the selected structural parameters of the case studied indicated that the airfoil shape has marginal effect on stability. In part II, flutter boundaries for a cascade of stator blade airfoils are presented for various values of structural and geometric parameters. Such a parametric study will allow general conclusions to be drawn about the effect of airfoil shape on aeroelastic stability of supersonic flow cascades.

ACKNOWLEDGEMENTS

The authors acknowledge Mr. John Ramsey for providing the linear theory program. This work was supported by NASA grants NAG3-1137, NAG3-1234, and NAG3-983.

REFERENCES

(1) Strack, W. C.; and Morris Jr., S. J.: The Challenges and Opportunities of Supersonic Transport Propulsion Technology. NASA TM 100921, 1988.

(2) Wood, J. R. et al: Application of Advanced Computational Codes in the Design of an Experiment for a Supersonic Throughflow Fan rotor. ASME Paper 87-GT-160.

(3) Ball, C. L.: Advanced Technologies Impact on Compressor Design and Development: A Perspective. NASA TM 102341, presented at Aerotech '89, Society of Automative Engineers, Anaheim, CA, Sept. 25-28, 1989.

(4) Lane, F.: Supersonic Flow Past an Oscillating Cascade with Supersonic Leading- Edge Locus. J. of Aeronaut. Sci., vol. 24, 1957, pp. 65-66.

(5) Platzer, M. F.; and Chalkley, Lt. H. G.: Theoretical Investigation of Supersonic Cascade Flutter and Related Interference Problems. AIAA Paper 72-377, 1972.

(6) Nishiyama, T.; and Kikuchi, M.: Theoretical Analysis for Unsteady Characteristics of Oscillating Cascade Aerofoils in Supersonic Flows. The Technology Reports of the Tohoku University, vol. 38, no. 2, 1973, pp 565-597.

(7) Nagashima, T.; and Whitehead, D. S.: Linearized Supersonic Unsteady Flow in Cascades. British ARC R & M 3811, 1977.

(8) Kielb, R. E.; and Ramsey, J. K.: Flutter of a Fan Blade in Supersonic Axial Flow. J. Turbomach., vol. 111, no.4, October 1989, pp. 462-467.

(9) Kaza, K. R. V.; and Kielb, R. E.: Flutter and Response of a Mistuned Cascade in Incompressible Flow. AIAA J., vol. 20, no. 8, Aug. 1982, pp. 1120-1127.

(10) Ramsey, J. K.: Influence of Thickness and Camber on the Aeroelastic Stability of Supersonic Throughflow Fans. J. Propulsion and Power, vol. 7, no. 3, May-June, 1991, pp. 404-411.

(11) Chima, R. V.: Explicit Multigrid Algorithm for Quasi-Three Dimensional Viscous Flows in Turbomachinery. J. of Propulsion and Power, vol. 3, no. 5, Sept-Oct. 1987, pp 397-405.

(12) Kao, Y. F.: A Two-Dimensional Unsteady Analysis for Transonic and Supersonic Cascade Flows. Ph.D. Thesis, School of Aeronautics and Astronautics, Purdue University, West Lafayette, Indiana, May 1989.

(13) Huff, D. L.; and Reddy, T. S. R.: Numerical Analysis of Supersonic Flow Through Oscillating Cascade Sections by Using a Deforming Grid. AIAA Paper 89-2805, 25th Joint Propulsion Conference, Monterey, CA, July 10-12, 1989

(14) Bakhle, M. A.; Reddy, T. S. R.; and Keith, T. G., Jr.: Time Domain Flutter Analysis of Cascades Using a Full-Potential Solver. AIAA J. vol. 20, no. 1,Jan. 1992, pp. 163-170.

(15) Reddy, T. S. R.; Bakhle, M. A.; and Huff, D. L.: Flutter Analysis of a Supersonic Cascade in Time Domain Using an ADI Euler Solver. NASA TM 105625, May 1992.

(16) Huff, D. L.; Swafford, T. W.; and Reddy, T. S. R.: Euler Flow Predictions for an Oscillating Cascade Using a High Resolution Wave-Split Scheme. ASME paper 91-GT-198, 1991 (also NASA TM 104377, 1991).

(17) Reddy, T. S. R.; Bakhle, M. A.; Huff, D. L.; and Swafford, T. W.: Flutter Analysis of Cascades Using a Two Dimensional Euler Solver. AIAA-91-1681, AIAA 22nd Fluid Dynamics, Plasma Dynamics & Lasers Conference, June 24-26, 1991, Honolulu, Hawaii.

(18) Bakhle, M. A.; Mahajan, A. J.; Keith, T. G. Jr.; and Stefko, G. L.: Cascade Flutter Analysis with Transient Response Aerodynamics. AIAA Paper 91-0747, 29th Aerospace Sciences Meeting, Jan, 1991.

(19) Whitfield, D. L.; Janus, J. M.; and Simpson, L. B.: Implicit Finite Volume High Resolution Wave-Split Scheme for Solving the Unsteady Three Dimensional Euler and Navier-Stokes Equations on Stationary or Dynamic Grids. Mississippi State Engineering and Industrial Research Station Report No. MSSU-EIRS-ASE-88-2, February, 1988.

(20) Roe, P. L.: Approximate Riemann Solvers, Parameter Vectors, and Difference Schemes. J. Computational Physics, vol. 43, 1981, pp. 357-372.

(21) Beam, R. M.; and Warming, R. F.: An Implicit Factored Scheme for the Compressible Navier-Stokes Equations. AIAA J.,vol. 16, no. 4, Apr. 1978, pp 393-402.

(22) Steger, J. L.; and Warming, R. F.: Flux Vector Splitting of the Inviscid Gasdynamic Equations with Application to Finite Difference Methods. J. Computational Physics, vol. 40, no.2, 1981, pp. 263-293.

(23) Lane, F.: System Mode Shapes in the Flutter of Compressor Blade Rows. J. Aeronaut. Sci., vol. 23, Jan. 1956, pp. 54-66.

(24) Bölcs, A.; Fransson, T. H.; and Schlafi, D.: Aerodynamic Superposition Principle in Vibrating Turbine Cascades. AGARD-CP-468, 1988, pp. 5.1-5.20.

Table I: Computational costs for HO, IC and PR+IC methods

Calculation method	Total computational time
HO method	$N_\sigma \;*\; N_{kb} \;*\; T_2$
IC method	$1 \;*\; N_{kb} \;*\; 2T_2$
PR+IC method	$1 \;*\; 1 \;*\; 2T_2$

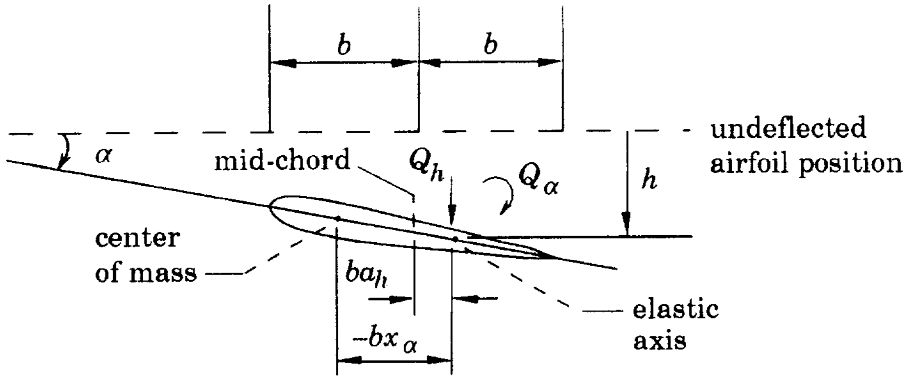

Figure 1: Typical section blade model with two degrees-of-freedom.

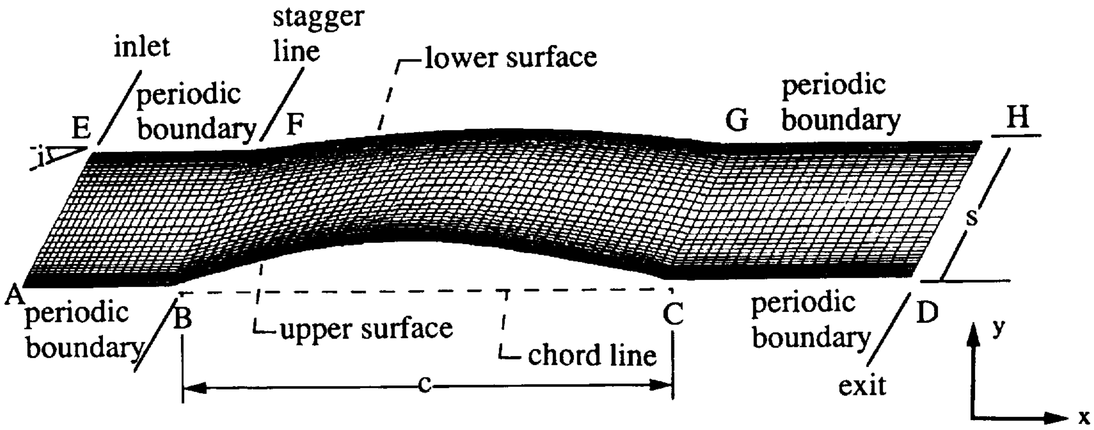

Figure 2a: Cascade geometry and grid for one blade passage.

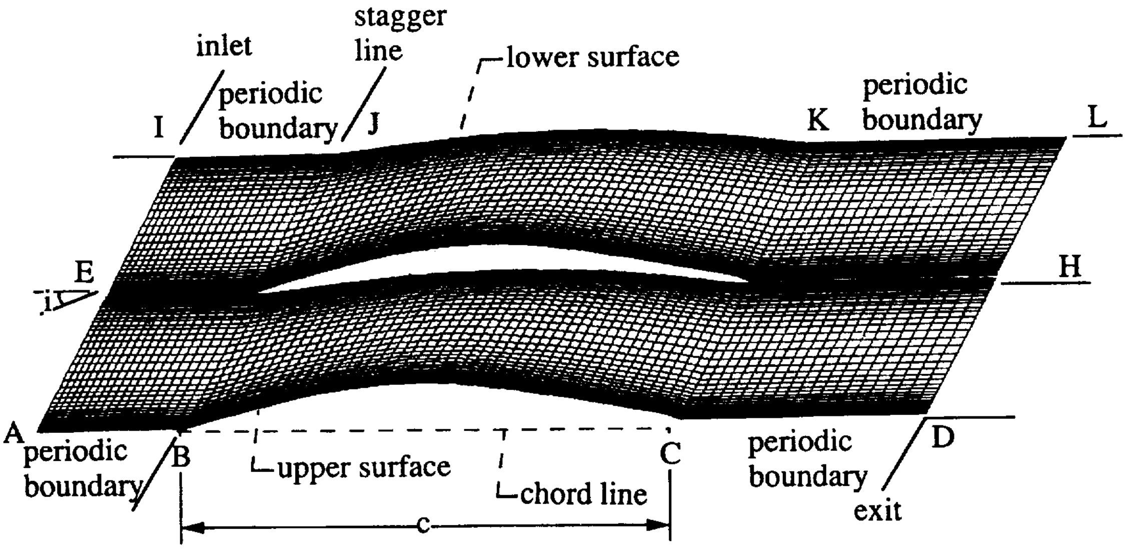

Figure 2b: Cascade geometry and grid for two blade passages.

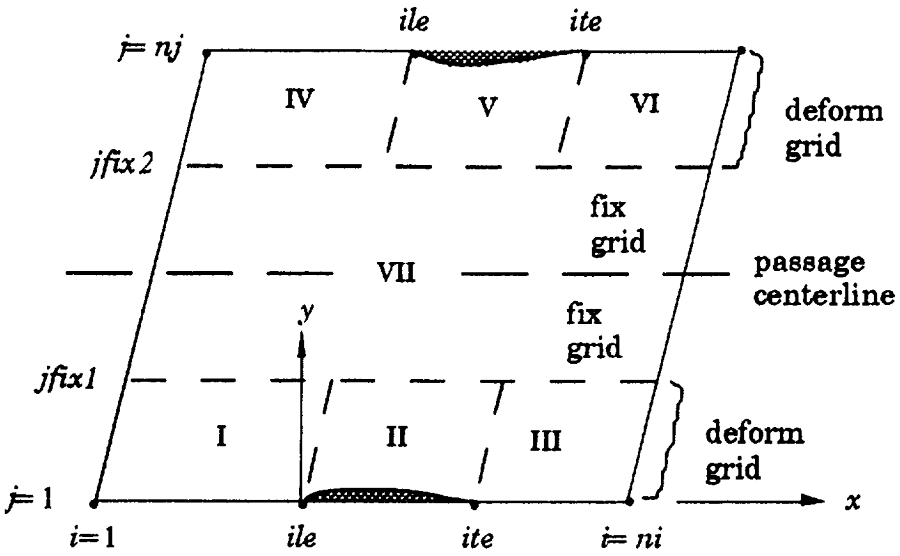

Figure 2c: Sub-blocking used for deforming the grid.

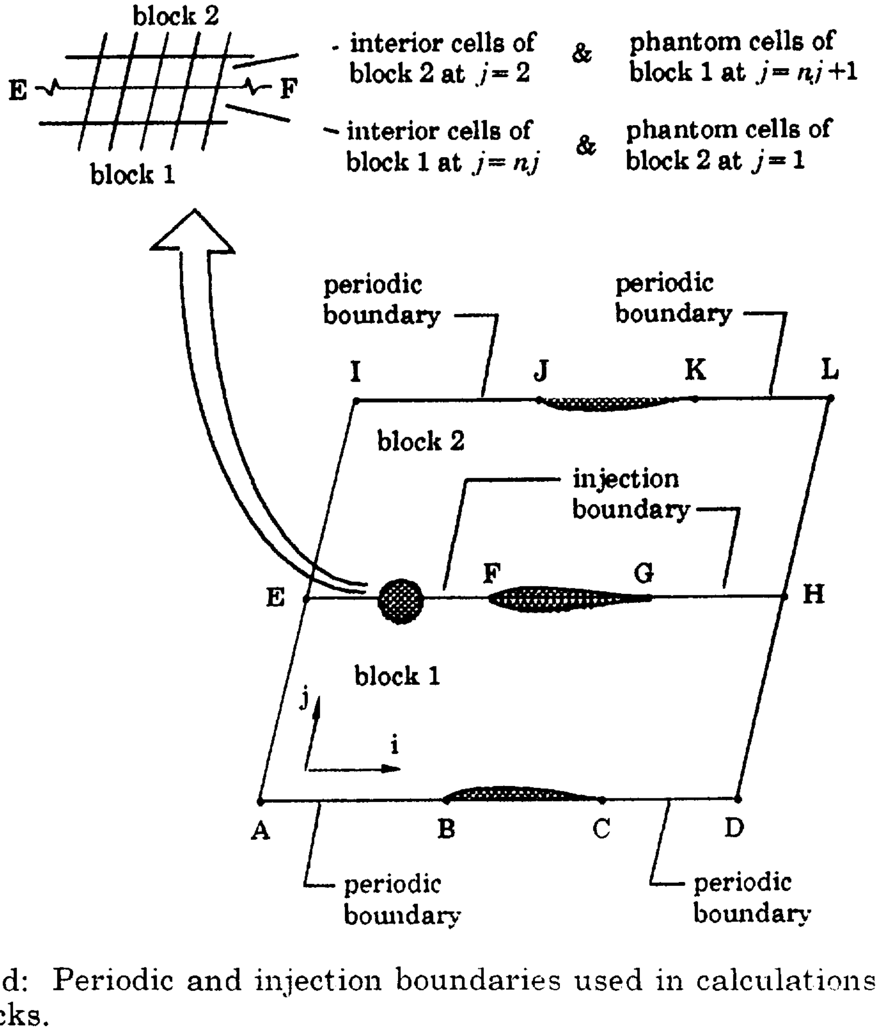

Figure 2d: Periodic and injection boundaries used in calculations with multiple grid blocks.

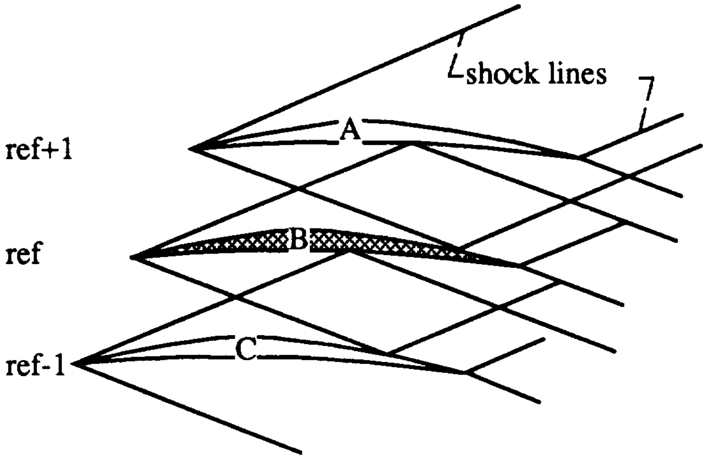

Fig. 3. Cascade in supersonic axial flow

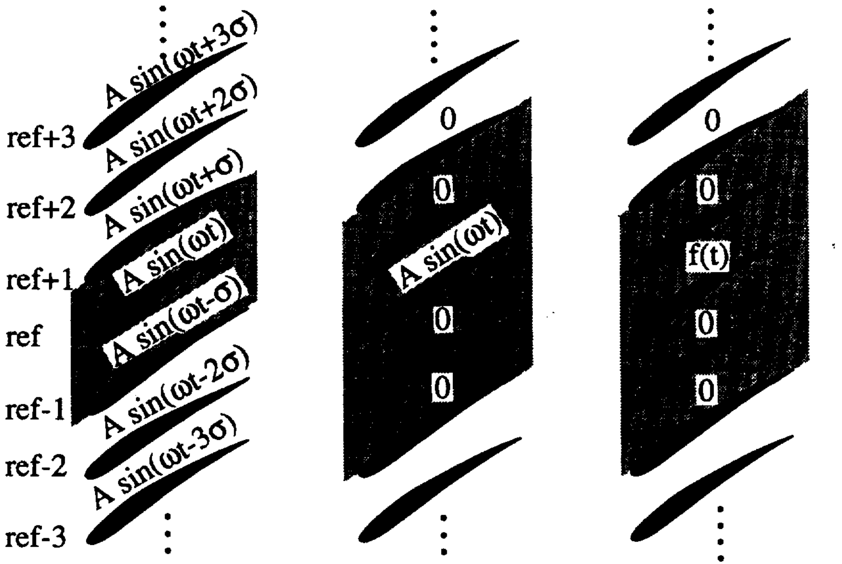

(a) Harmonic Oscillation (HO)

(b) Influence Coefficient (IC)

(c) Pulse Response (PR)

Fig. 4: Setup showing number of blocks used in computation with blade motion as indicated.

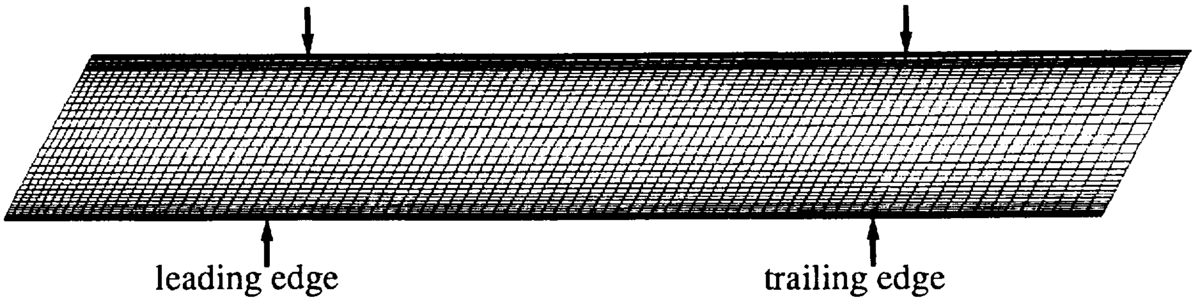

Fig. 5: Flat plate grid (91×41)

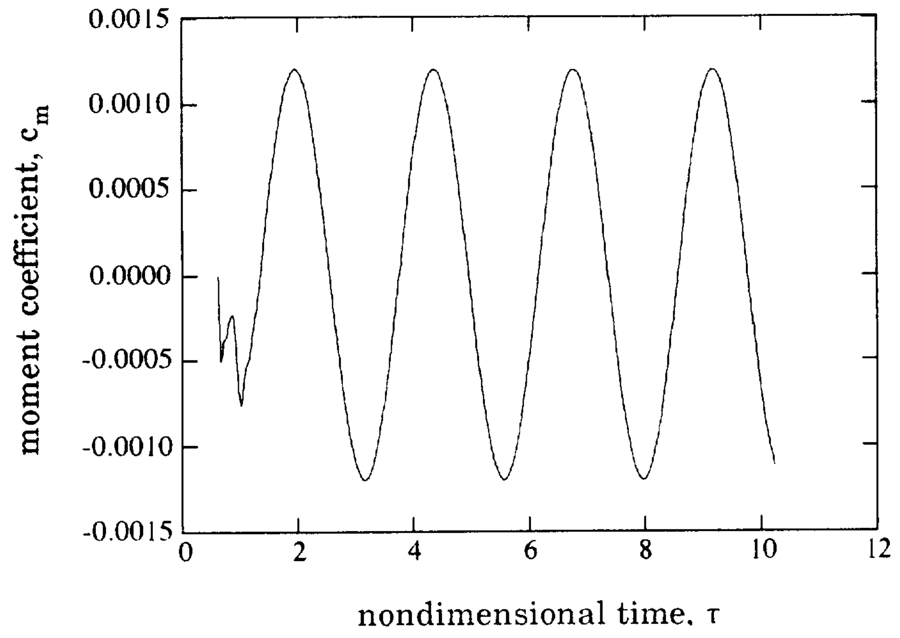

Fig. 6a: Moment coefficient vs. time in pitching motion, $k_b = 0.5$, $\sigma = 180$ deg, $\alpha_o = 0.1$ deg.

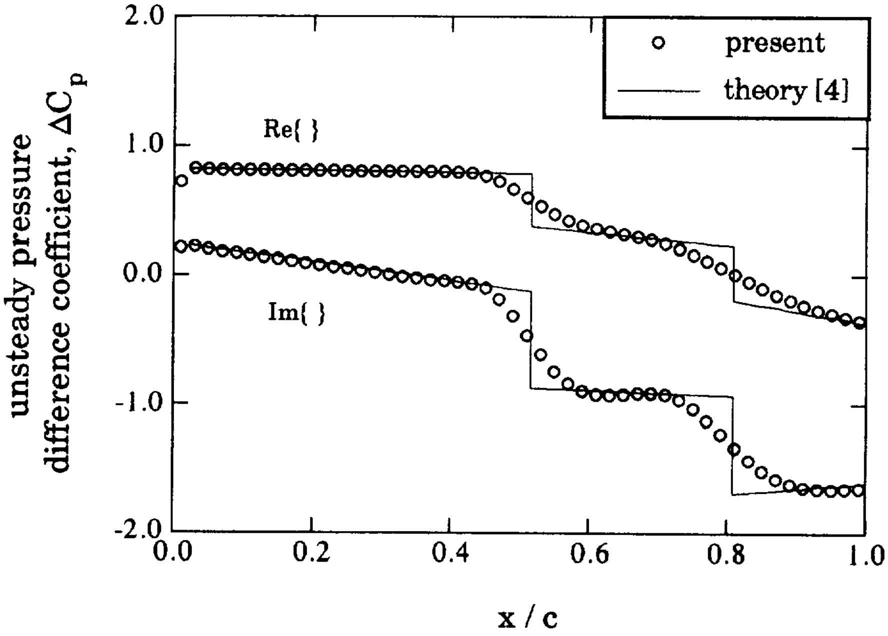

Fig. 6b: Unsteady pressure difference distribution, $\sigma = 0$ deg, $k_b = 0.5$, pitching.

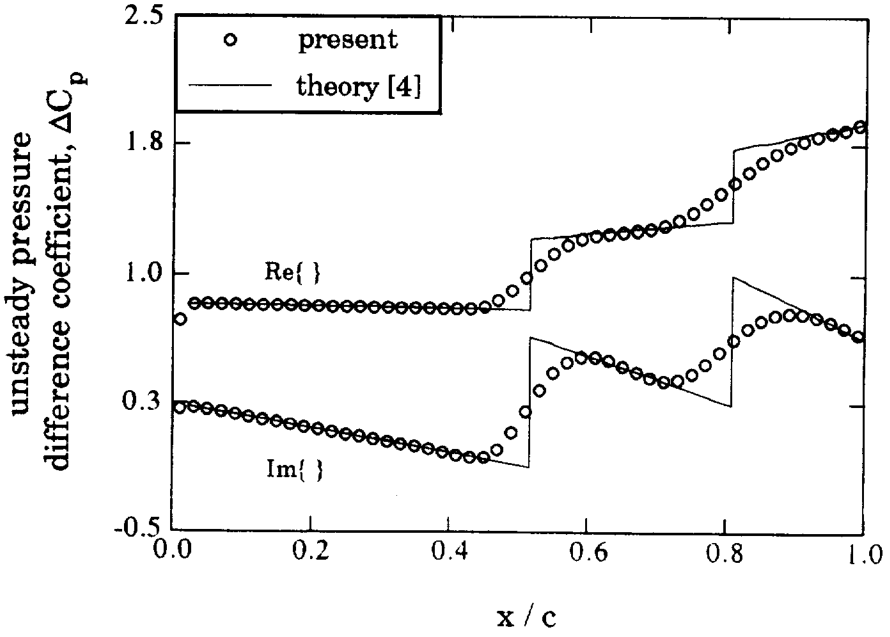

Fig. 6c: Unsteady pressure difference distribution, $\sigma = 180$ deg, $k_b = 0.5$, pitching.

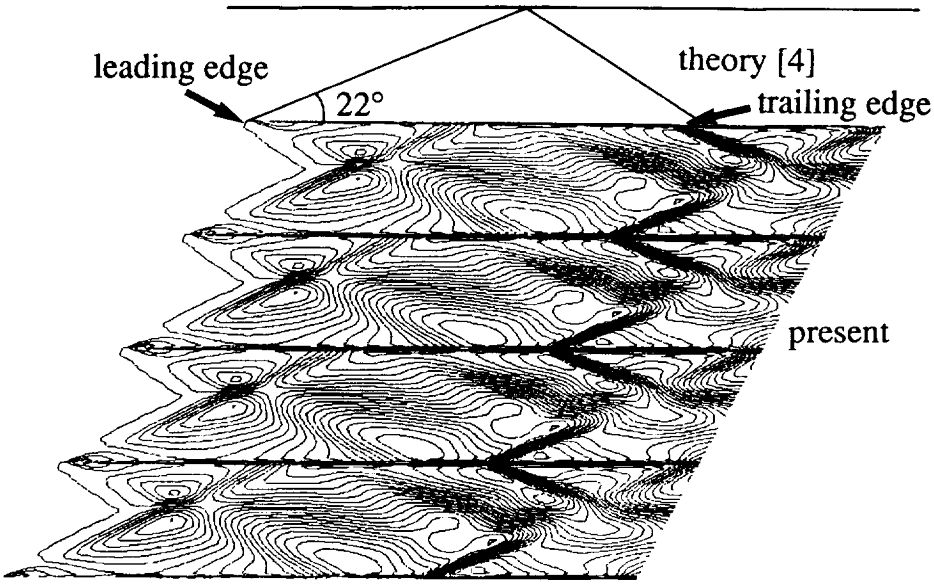

Fig. 6d: Instantaneous Mach contours for pitching flat plate cascade

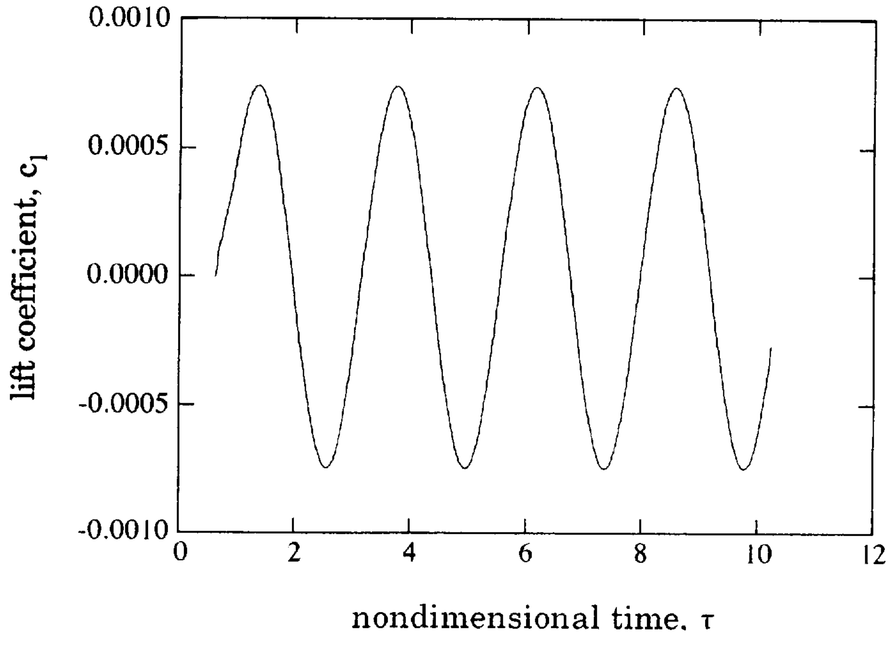

Fig. 7a: Lift coefficient vs. time in plunging motion, $k_b = 0.5$, $\sigma =$ 180 deg, $h_o/c = 0.0003$.

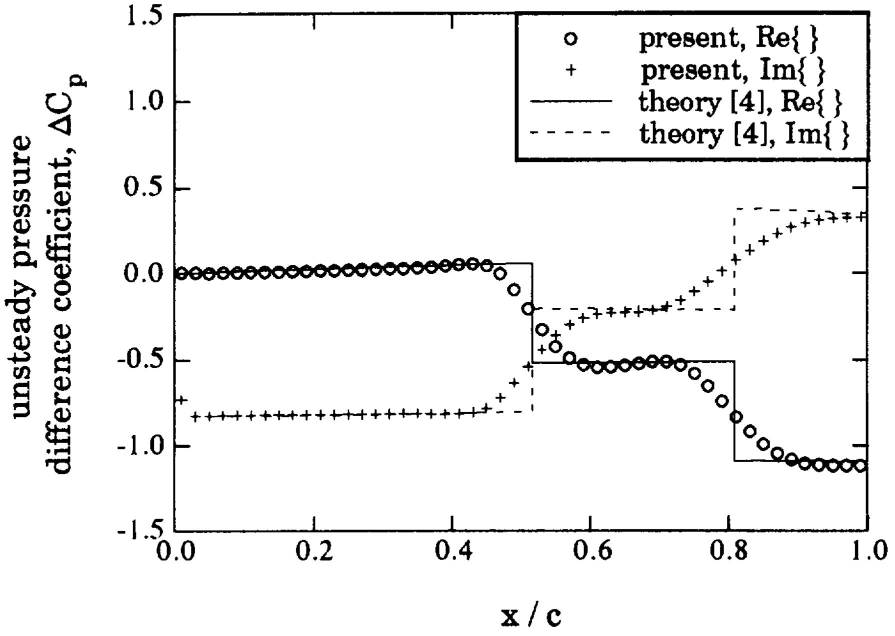

Fig. 7b: Unsteady pressure difference distribution, $\sigma = 0$ deg, $k_b = 0.5$, plunging.

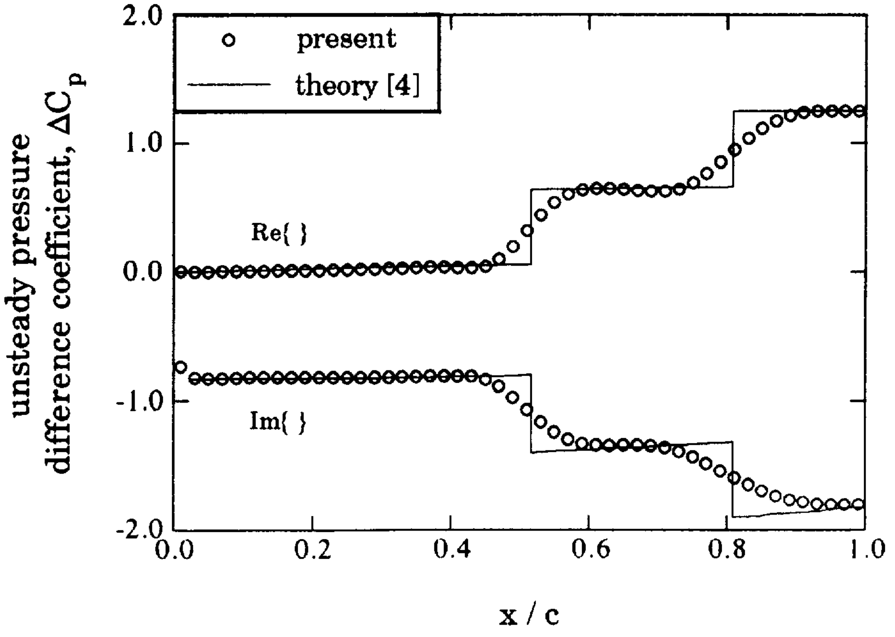

Fig. 7c: Unsteady pressure difference distribution, $\sigma = 180$ deg, $k_b = 0.5$, plunging.

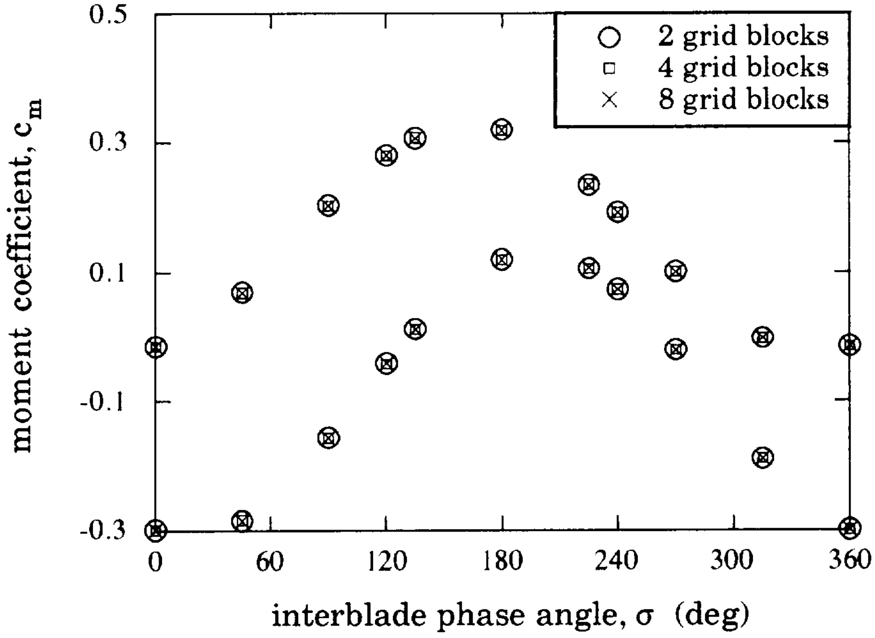

Fig. 8a: Comparison of moment coefficient with 2, 4 and 8 grid blocks, $k_b = 0.5$, pitching.

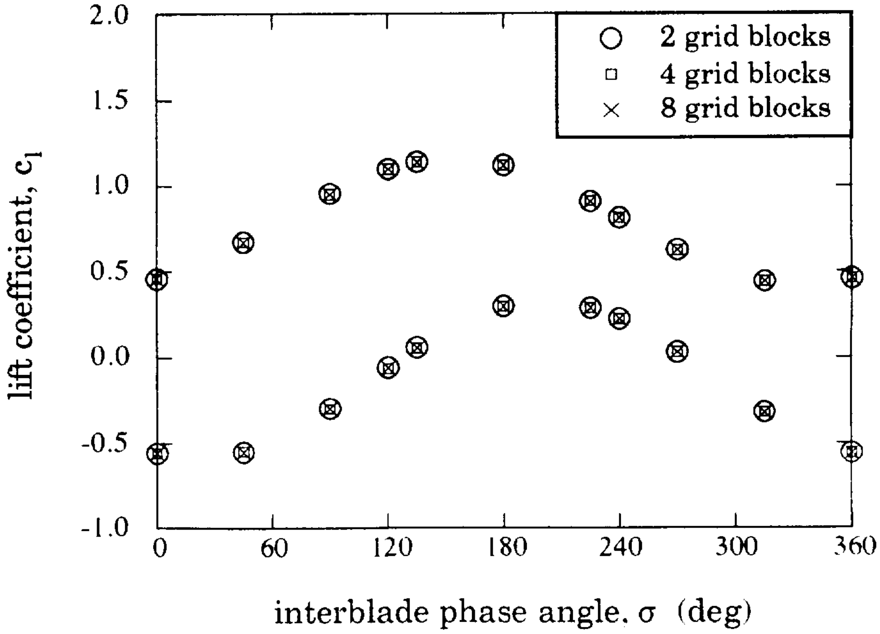

Fig. 8b: Comparison of lift coefficient with 2, 4 and 8 grid blocks, $k_b = 0.5$, pitching.

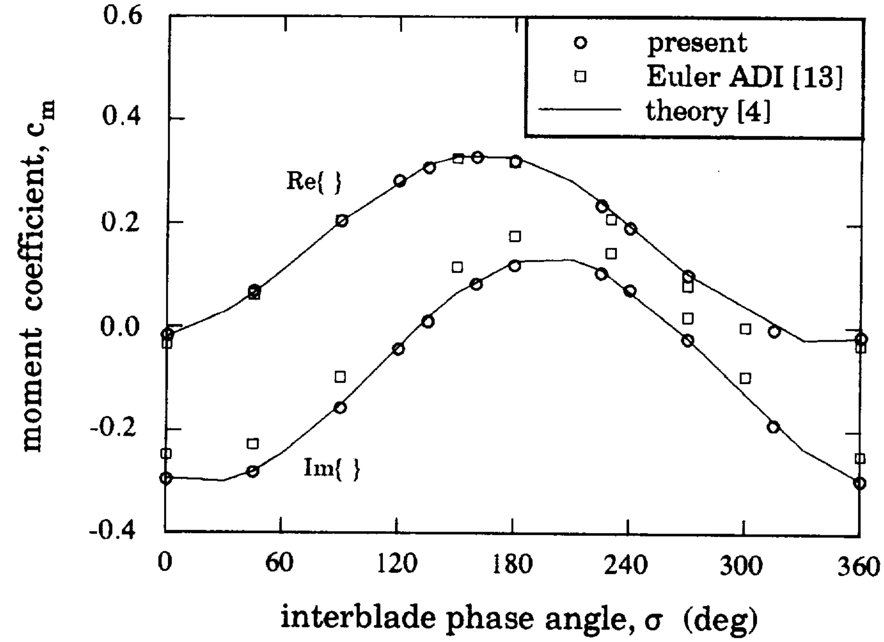

Fig. 9a: Variation of moment coefficient with phase angle, $k_b = 0.5$, pitching.

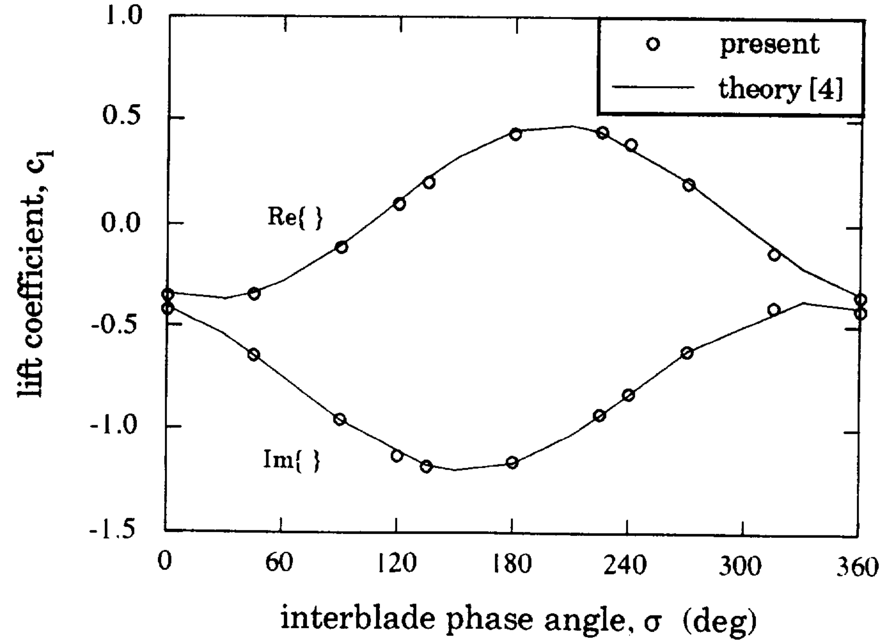

Fig. 9b: Variation of lift coefficient with phase angle, $k_b = 0.5$, plunging.

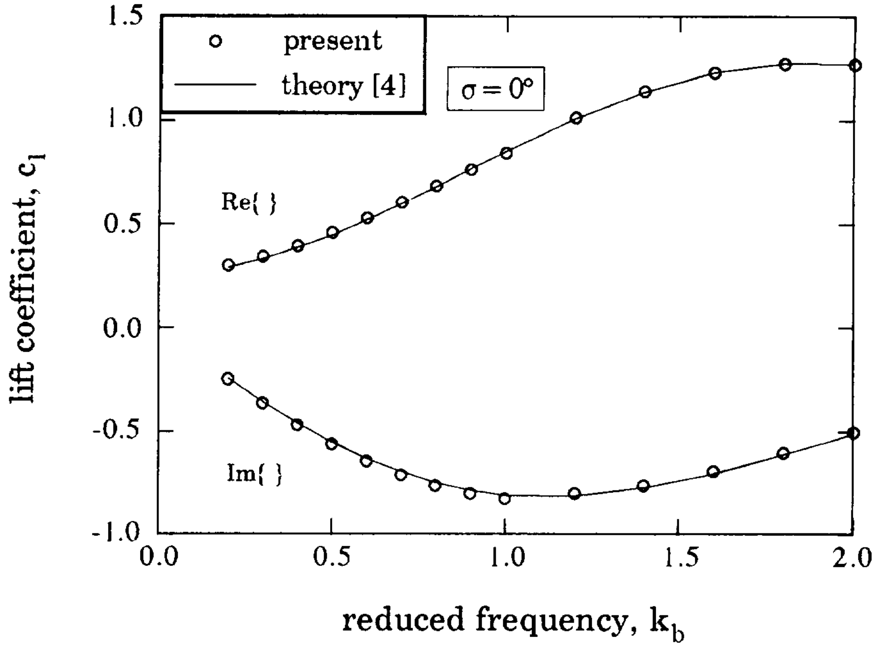

Fig. 10a: Variation of lift coefficient with reduced frequency, $\sigma = 0$ deg, pitching.

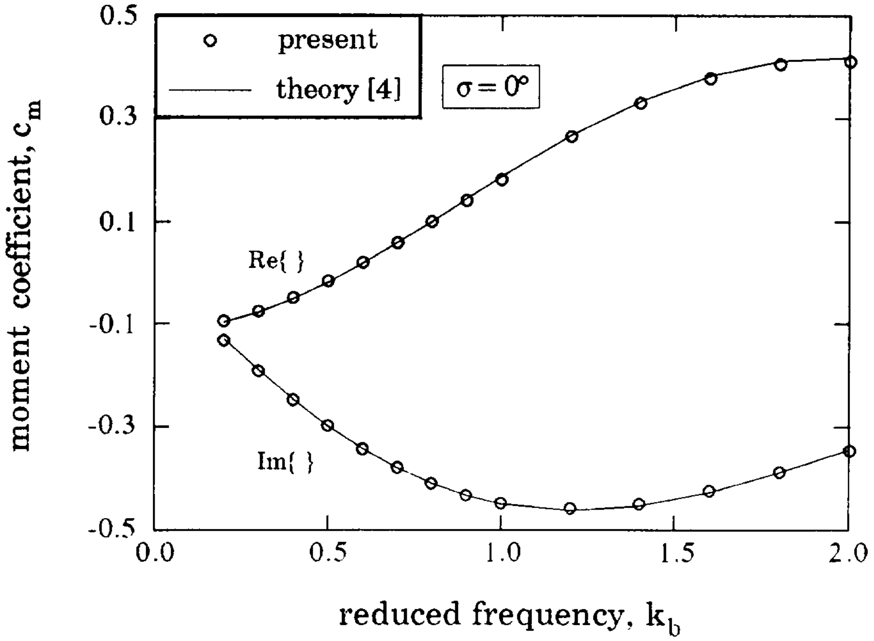

Fig. 10b: Variation of moment coefficient with reduced frequency, $\sigma = 0$ deg, pitching.

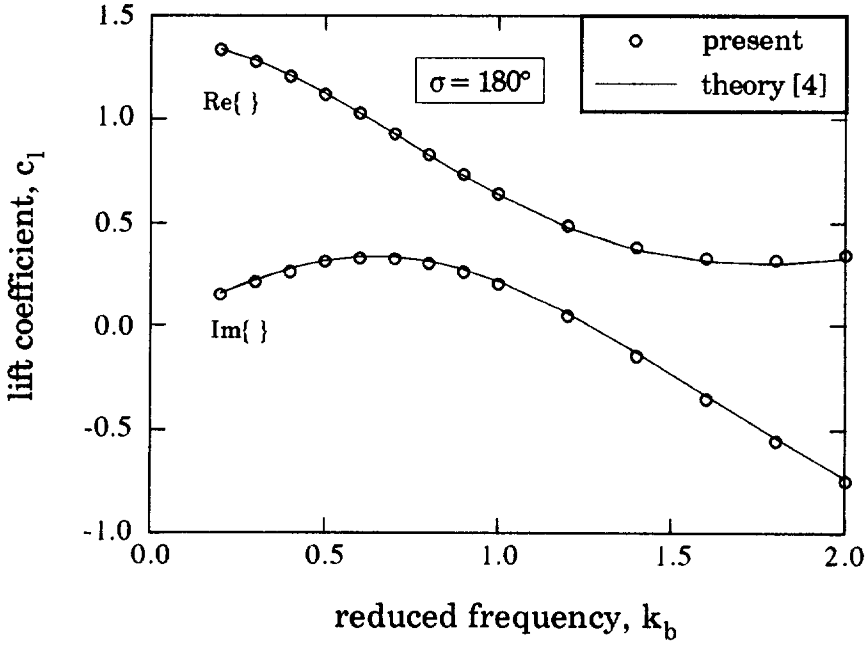

Fig. 10c: Variation of lift coefficient with reduced frequency, $\sigma = 180$ deg, pitching.

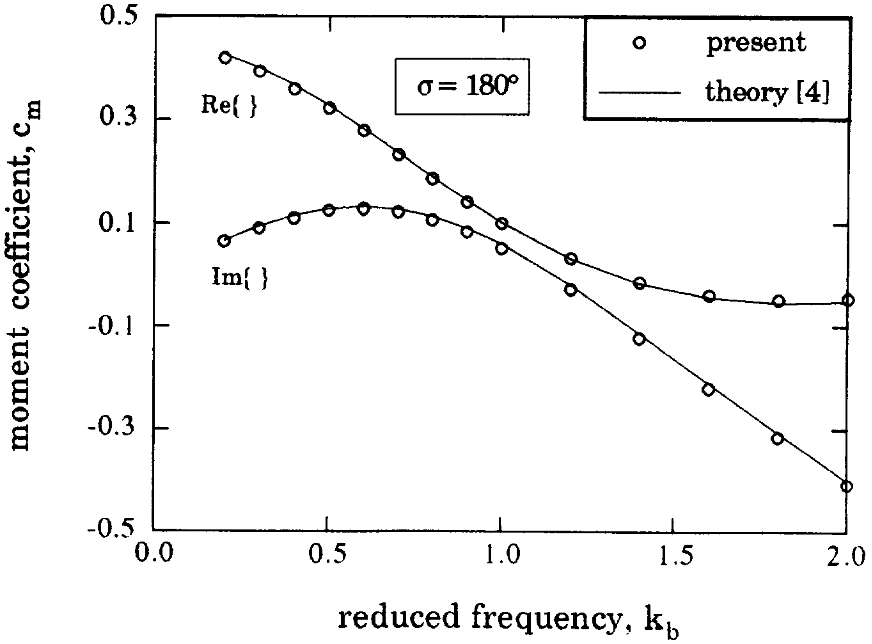

Fig. 10d: Variation of moment coefficient with reduced frequency, $\sigma = 180$ deg, pitching.

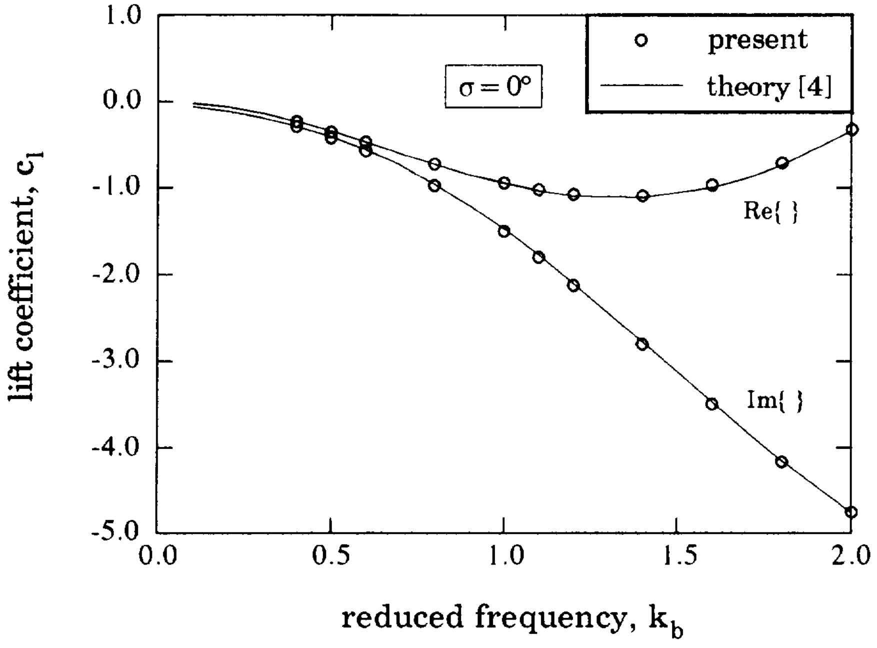

Fig. 11a: Variation of lift coefficient with reduced frequency, $\sigma = 0$ deg, plunging.

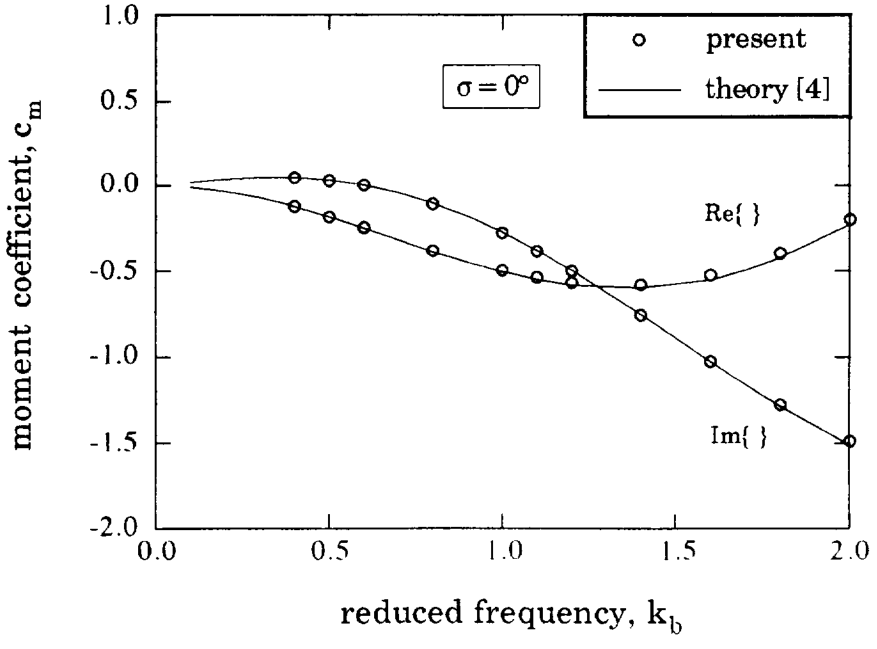

Fig. 11b: Variation of moment coefficient with reduced frequency, $\sigma = 0$ deg, plunging.

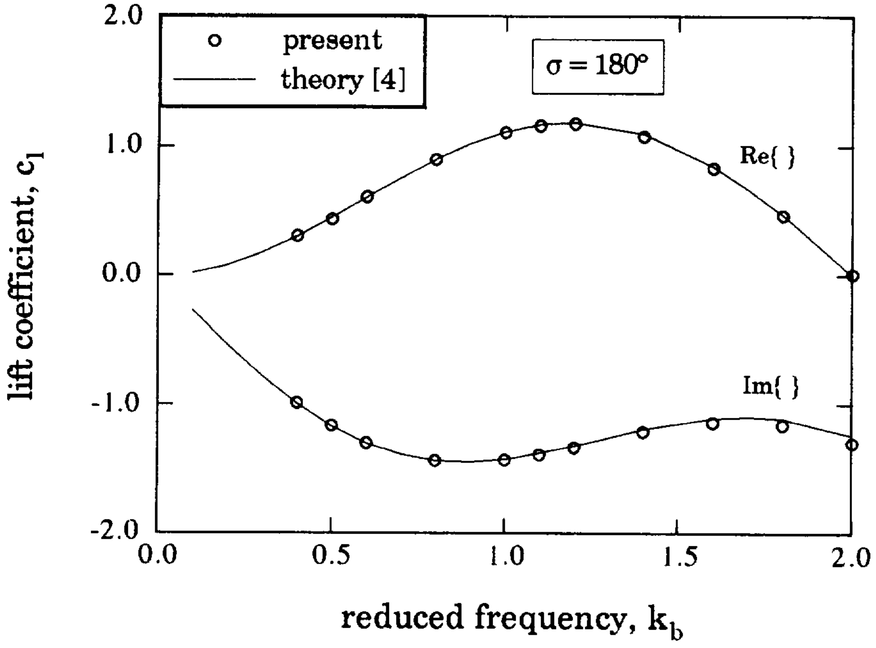

Fig. 11c: Variation of lift coefficient with reduced frequency, $\sigma = 180$ deg, plunging.

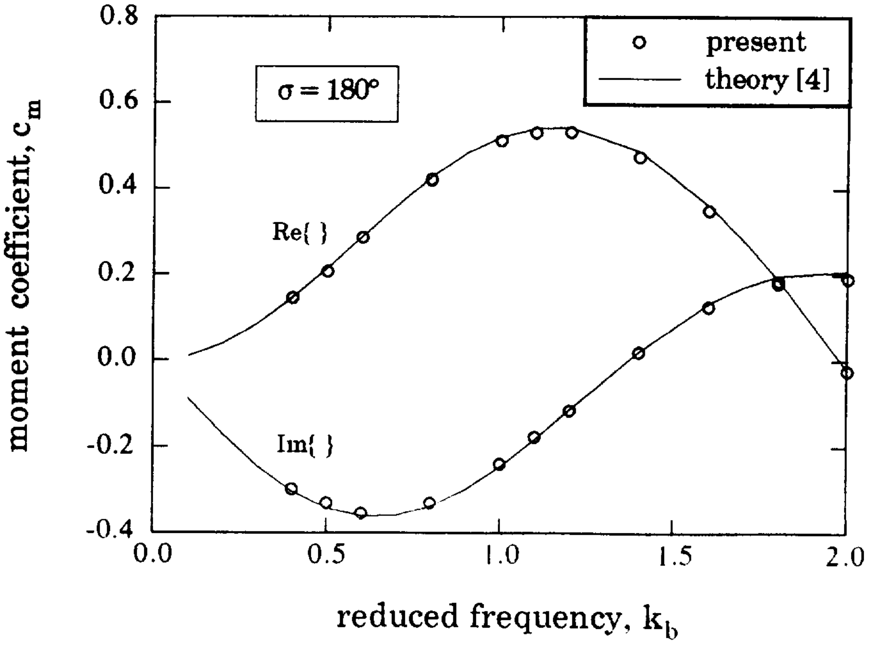

Fig. 11d: Variation of moment coefficient with reduced frequency, $\sigma = 180$ deg, plunging.

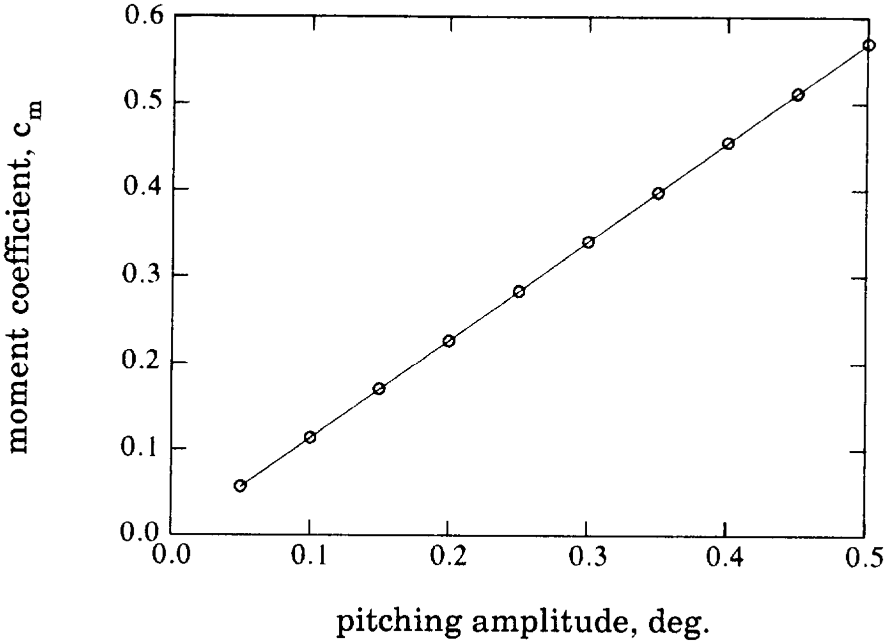

Fig. 11e Variation of moment coefficient with amplitude showing linear relationship, $k_b = 1.0$, $\sigma = 180$ deg.

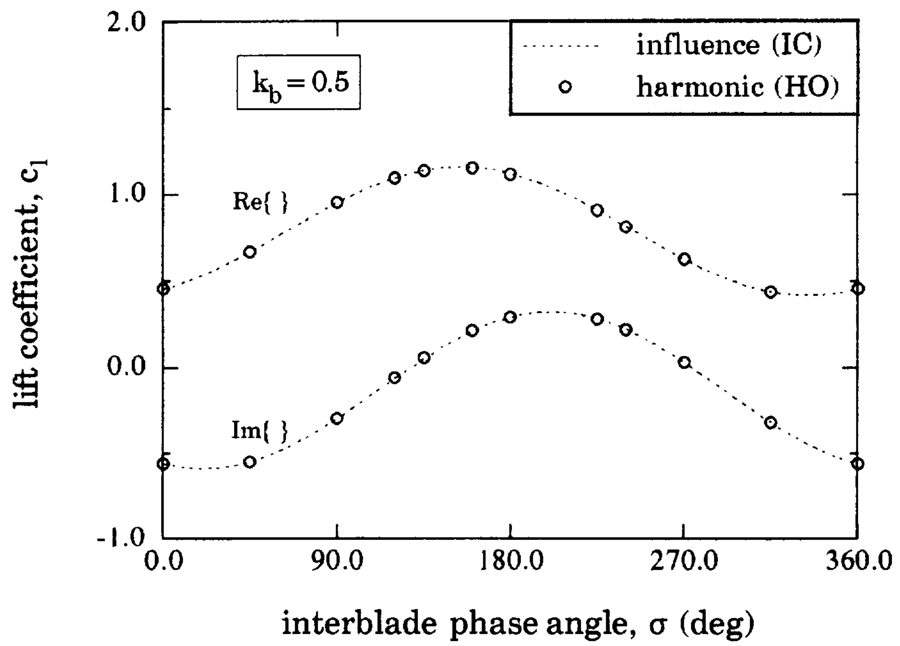

Fig. 12a: Comparison of lift coefficient from HO and IC methods, $k_b = 0.5$, pitching.

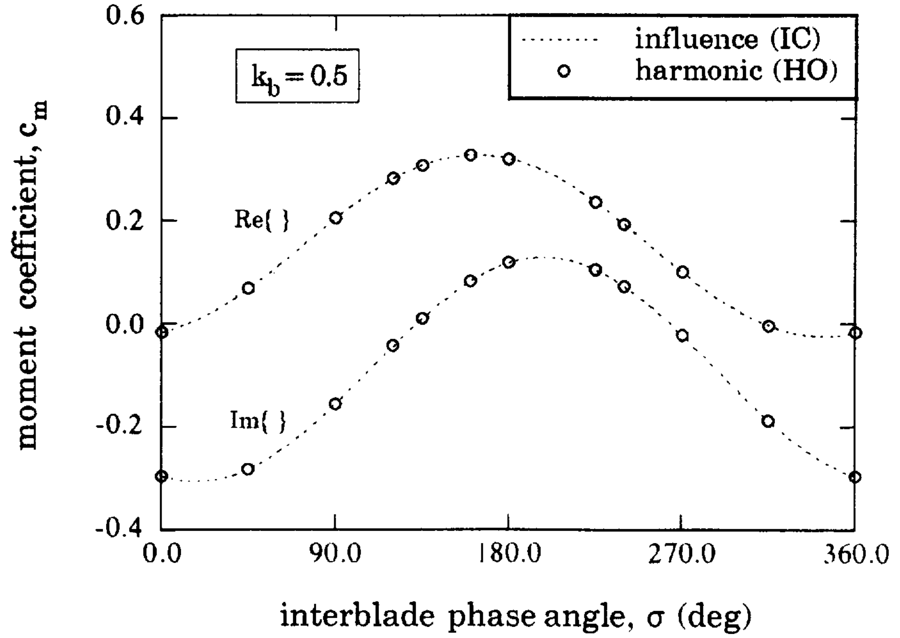

Fig. 12b: Comparison of moment coefficient from HO and IC methods, $k_b = 0.5$, pitching.

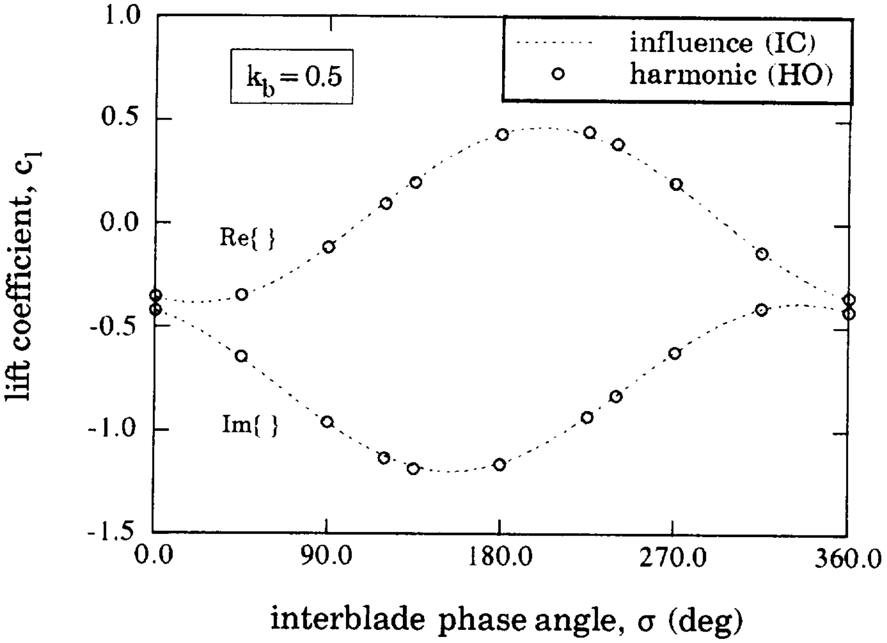

Fig. 13a: Comparison of lift coefficient from HO and IC methods, $k_b = 0.5$, plunging.

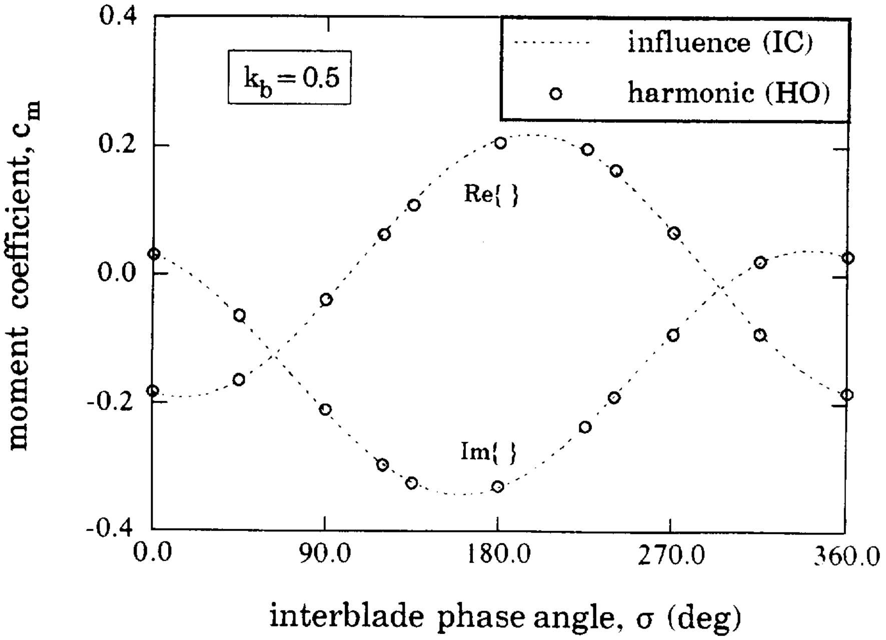

Fig. 13b: Comparison of moment coefficient from HO and IC methods, $k_b = 0.5$, plunging.

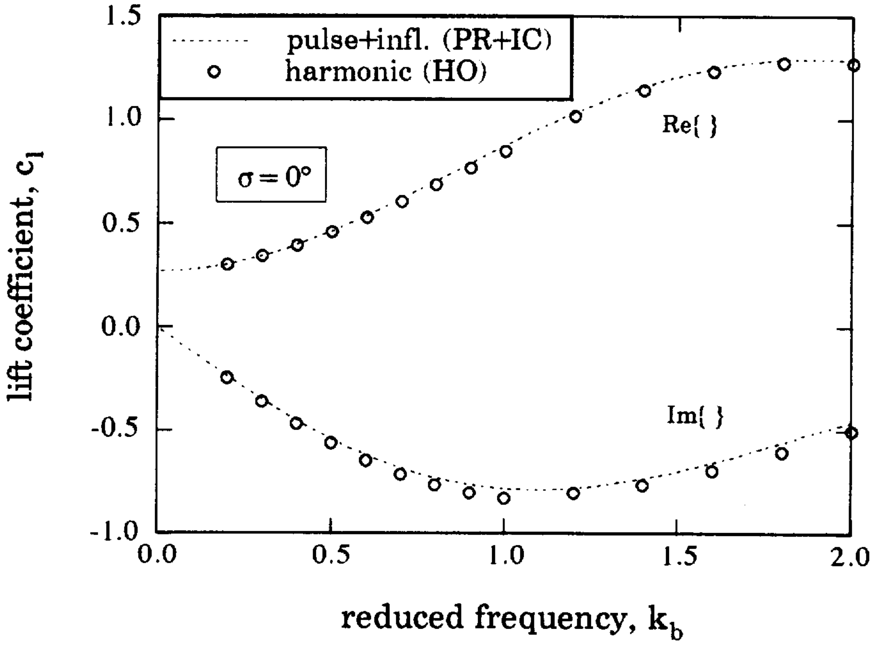

Fig. 14a: Comparison of lift coefficient from HO and PR methods, $\sigma = 0$ deg, pitching.

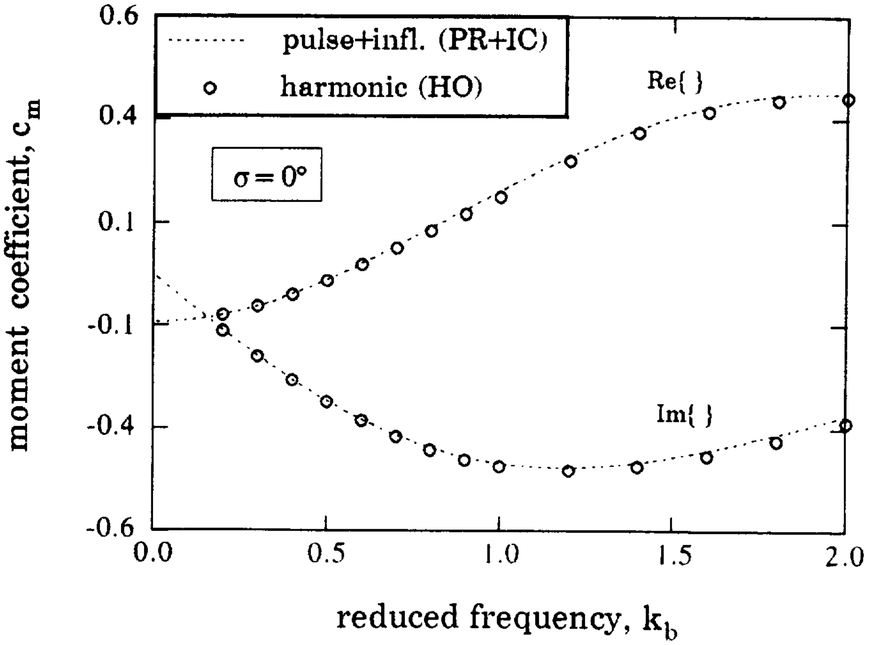

Fig. 14b: Comparison of moment coefficient from HO and PR methods, $\sigma = 0$ deg, pitching.

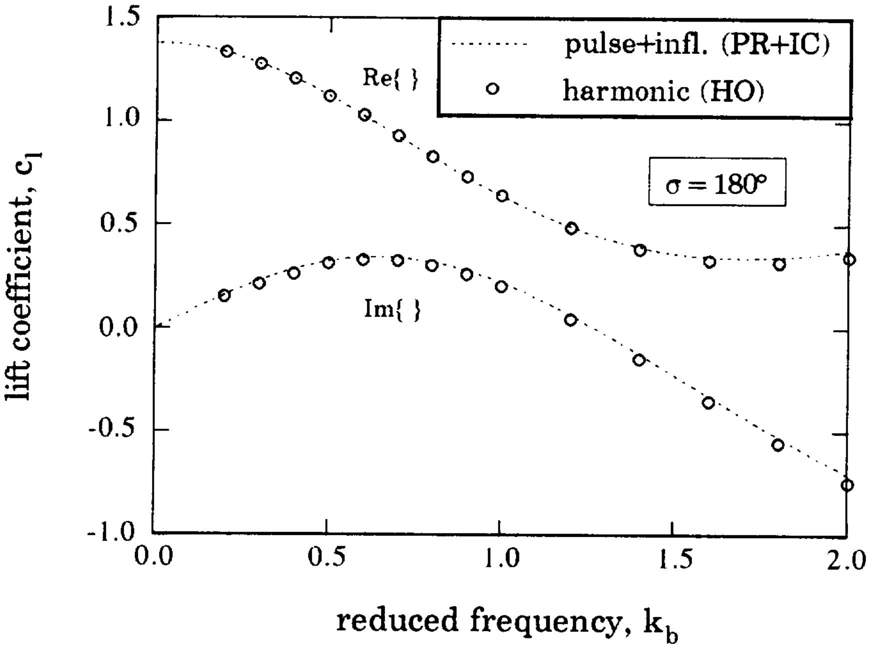

Fig. 14c: Comparison of lift coefficient from HO and PR methods, $\sigma = 180$ deg, pitching.

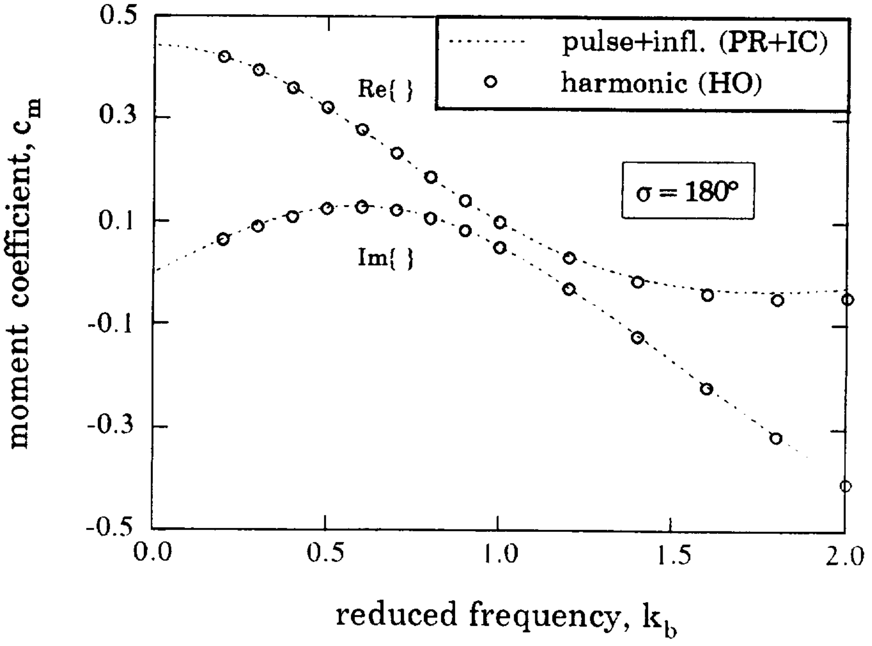

Fig. 14d: Comparison of moment coefficient from HO and PR methods, $\sigma = 180$ deg, pitching.

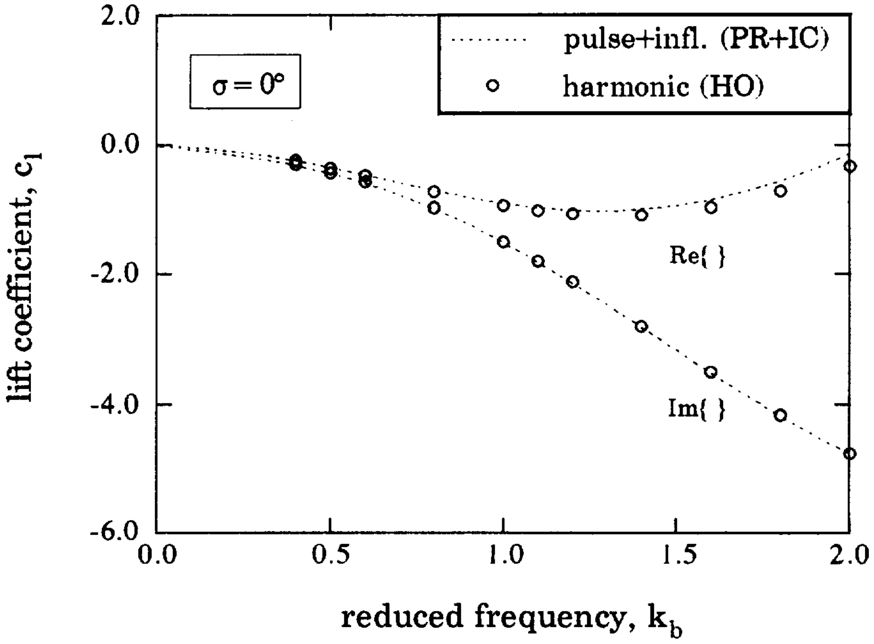

Fig. 15a: Comparison of lift coefficient from HO and PR methods, $\sigma = 0$ deg, plunging.

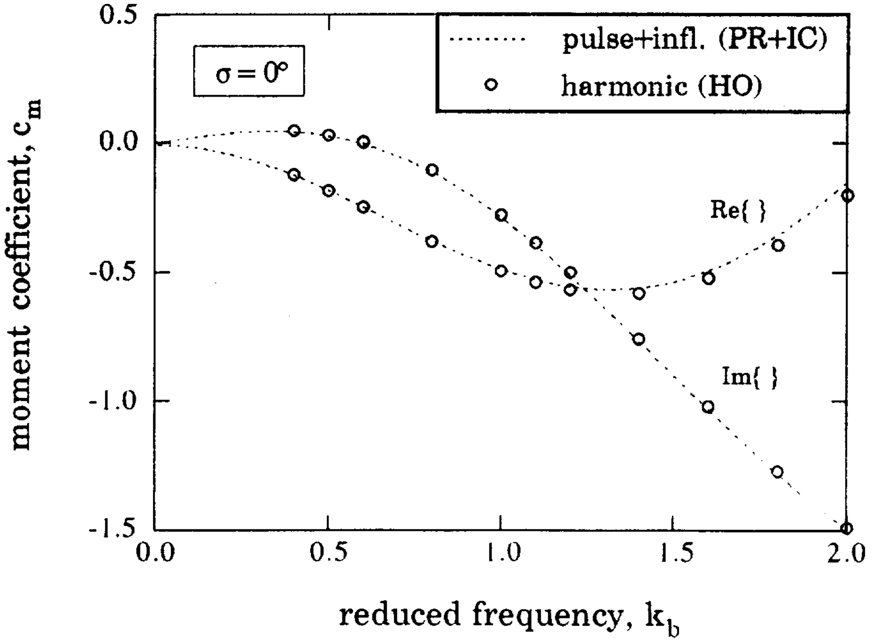

Fig. 15b: Comparison of moment coefficient from HO and PR methods, $\sigma = 0$ deg, plunging.

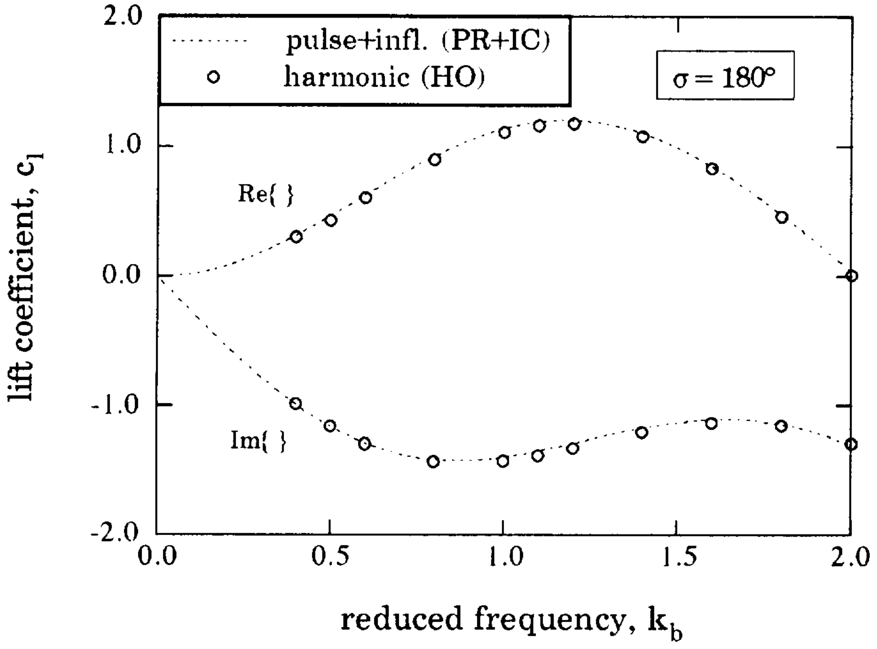

Fig. 15c: Comparison of lift coefficient from HO and PR methods, σ = 180 deg, plunging.

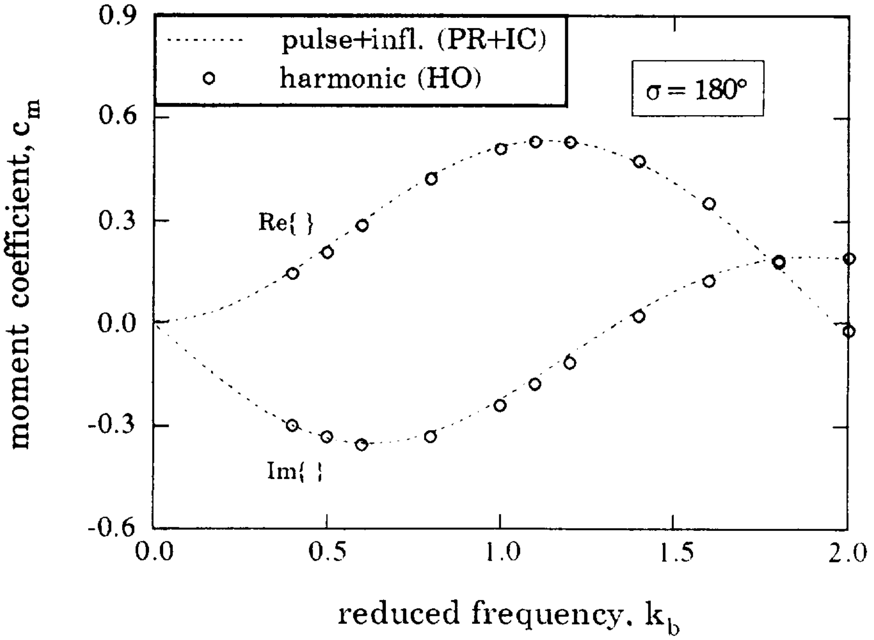

Fig. 15d: Comparison of moment coefficient from HO and PR methods, σ = 180 deg, plunging.

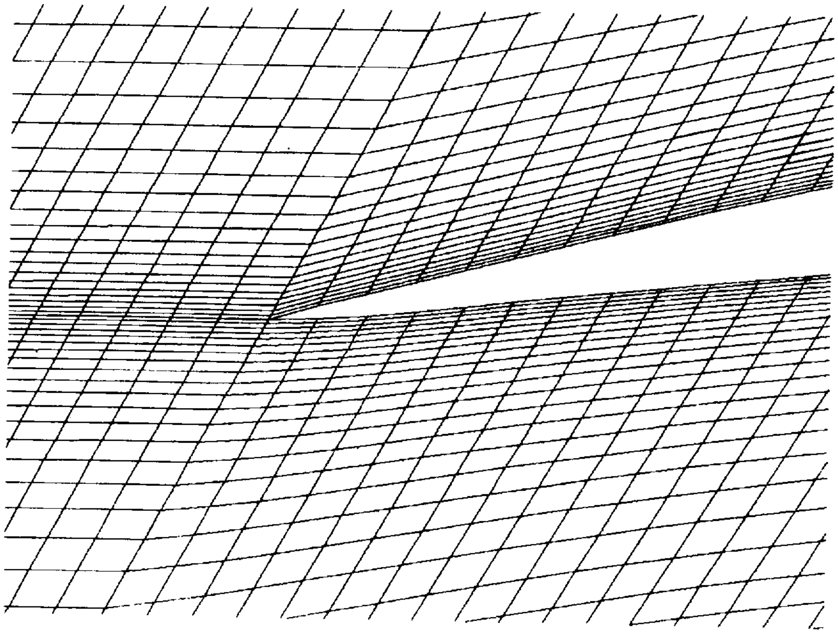

Fig. 16a: Grid near leading edge for the rotor airfoil .

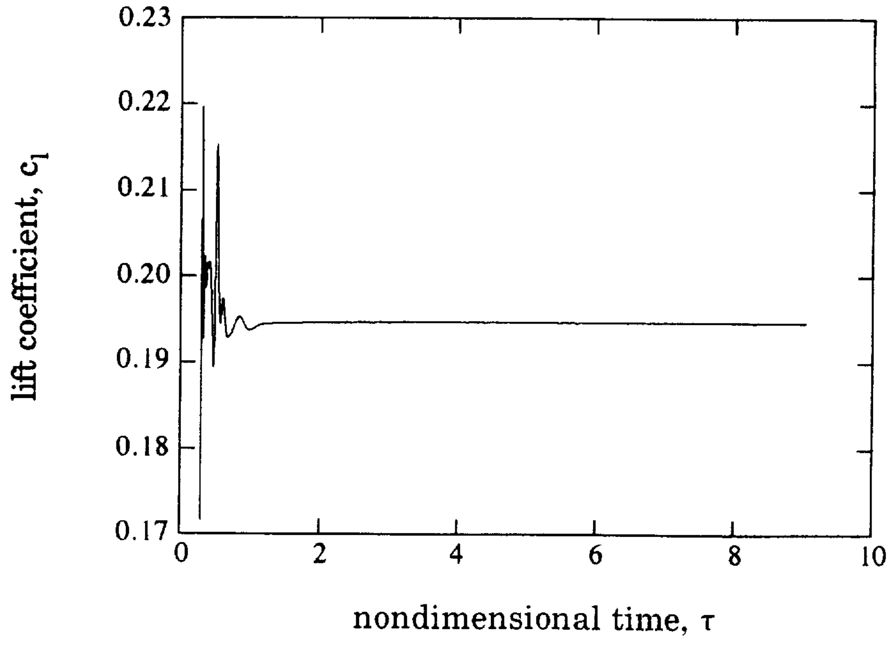

Fig. 16b: Convergence of the steady lift coefficient of the rotor airfoil cascade.

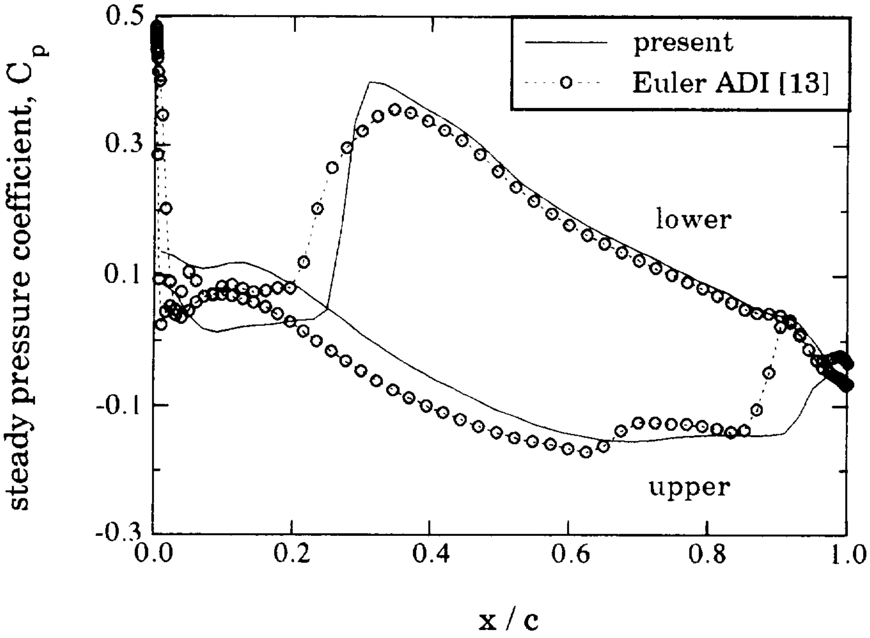

Fig. 16c: Comparison of steady pressure distribution of the rotor airfoil, present solver vs Ref. 13.

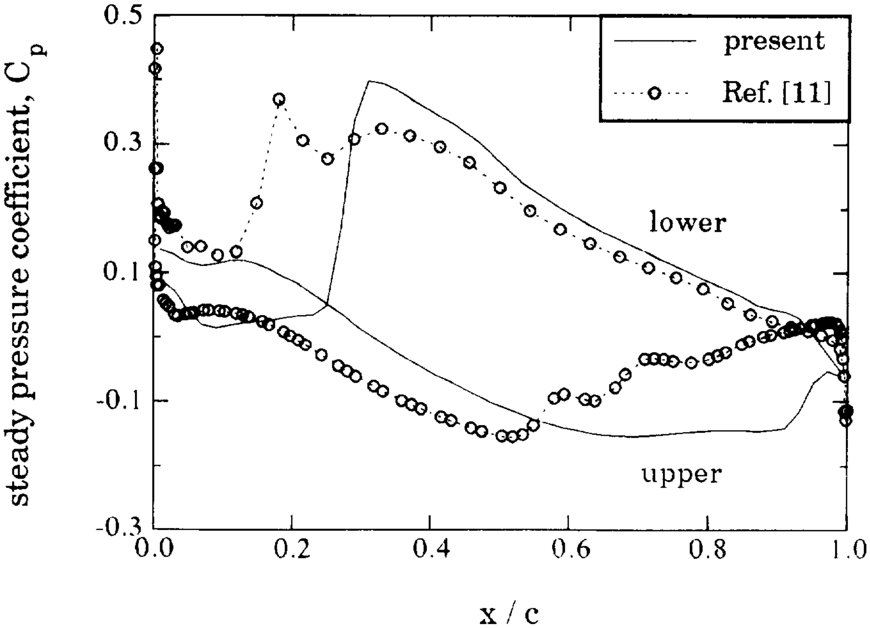

Fig. 16d: Comparison of steady pressure distribution of the rotor airfoil, present solver vs Ref. 11.

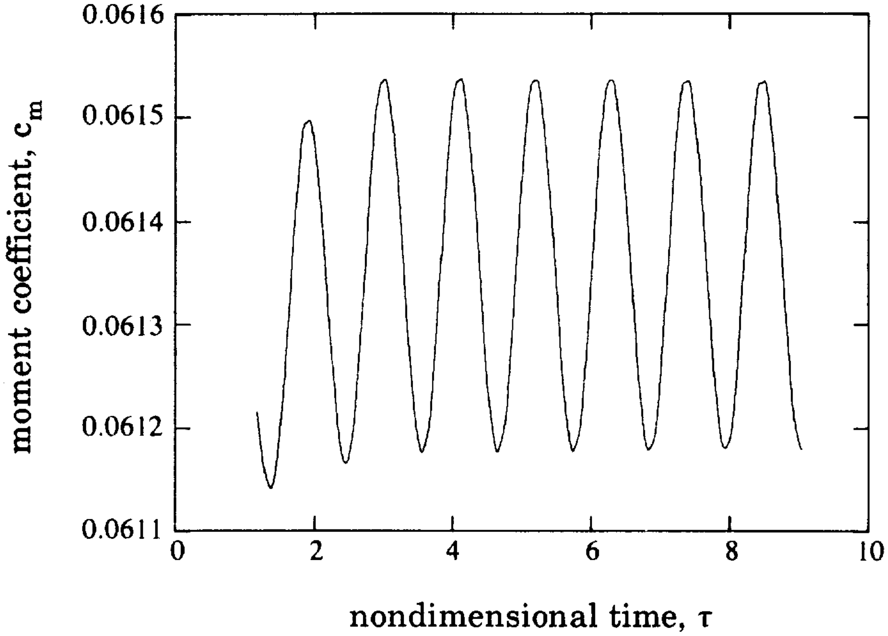

Fig. 17a: Moment coefficient vs. time in pitching motion, $k_b = 1.1$, $\sigma = 180$ deg, $\alpha_o = 0.1$ deg.

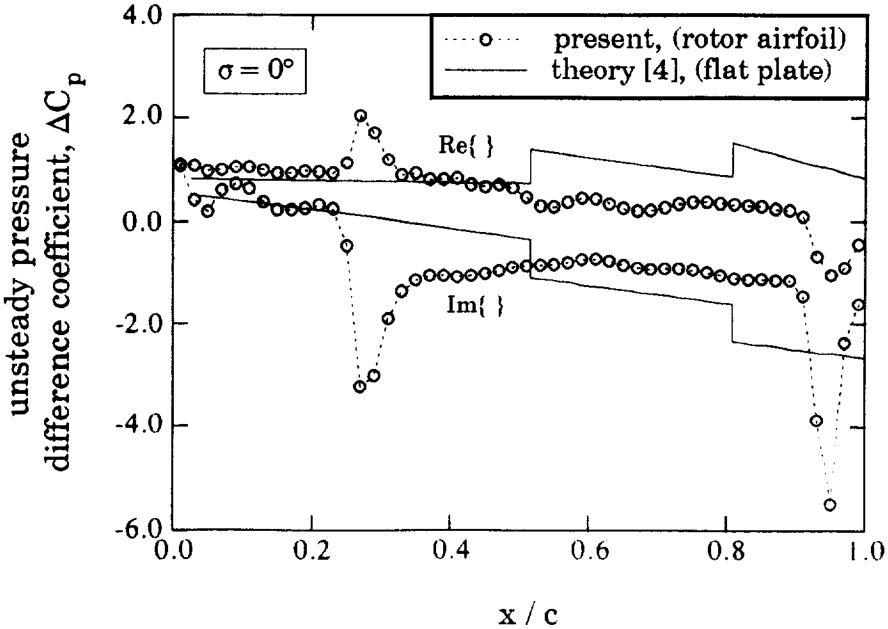

Fig. 17b: Unsteady pressure difference distribution, $\sigma = 0$ deg, $k_b = 1.1$, pitching.

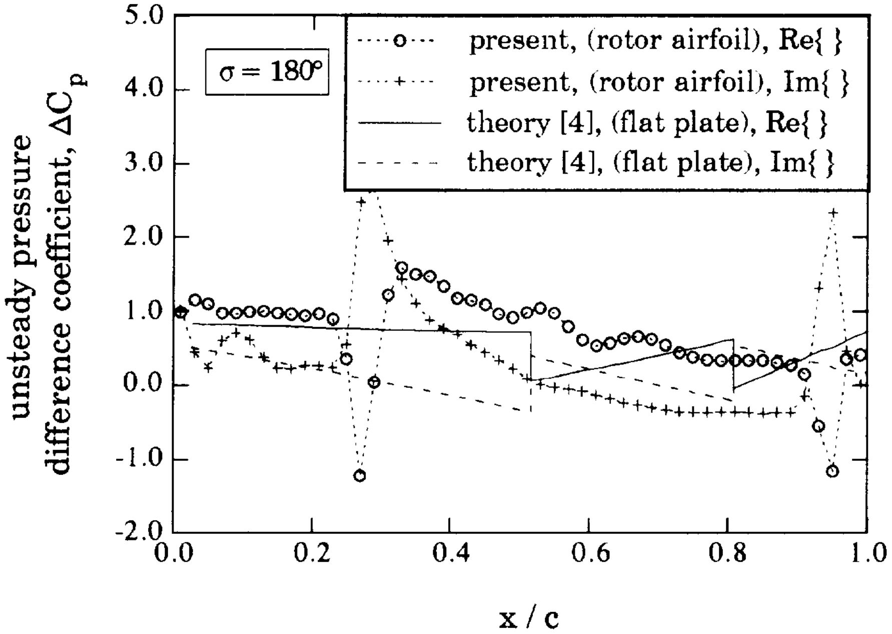

Fig. 17c: Unsteady pressure difference distribution, $\sigma = 180$ deg, $k_b = 1.1$, pitching.

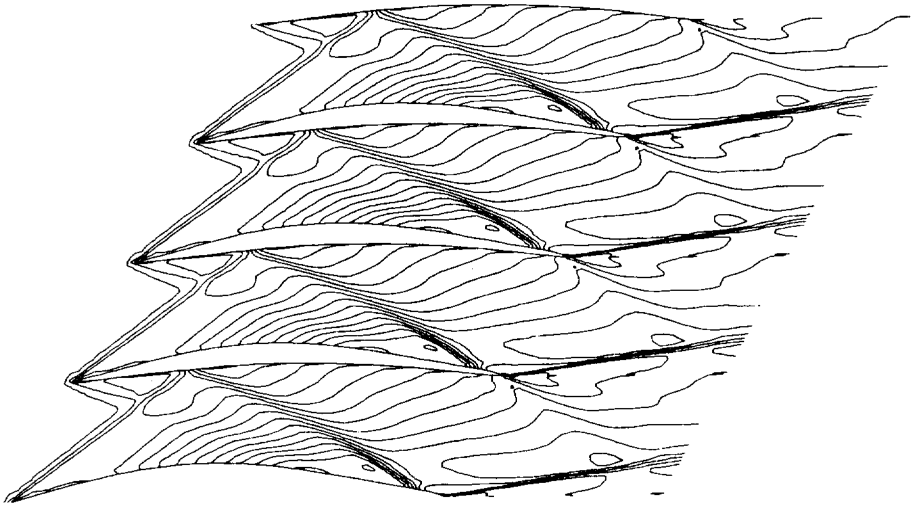

Fig. 17d: Instantaneous Mach contours for pitching rotor airfoil cascade

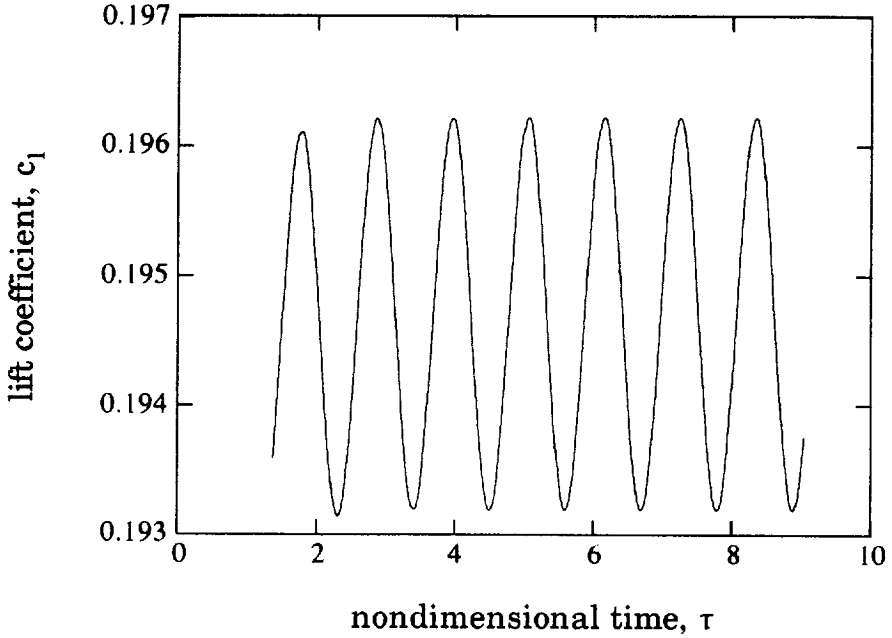

Fig. 18a: Lift coefficient vs. time in plunging motion, $k_b = 1.1$, $\sigma = 180$ deg, $h_o/c = 0.0003$.

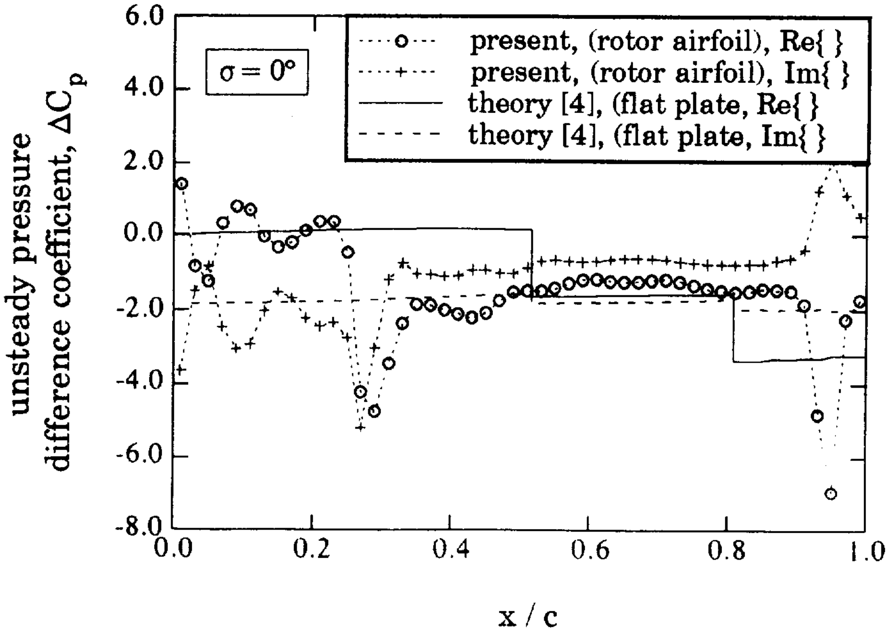

Fig. 18b: Unsteady pressure difference distribution, $\sigma = 0$ deg, $k_b = 1.1$, plunging.

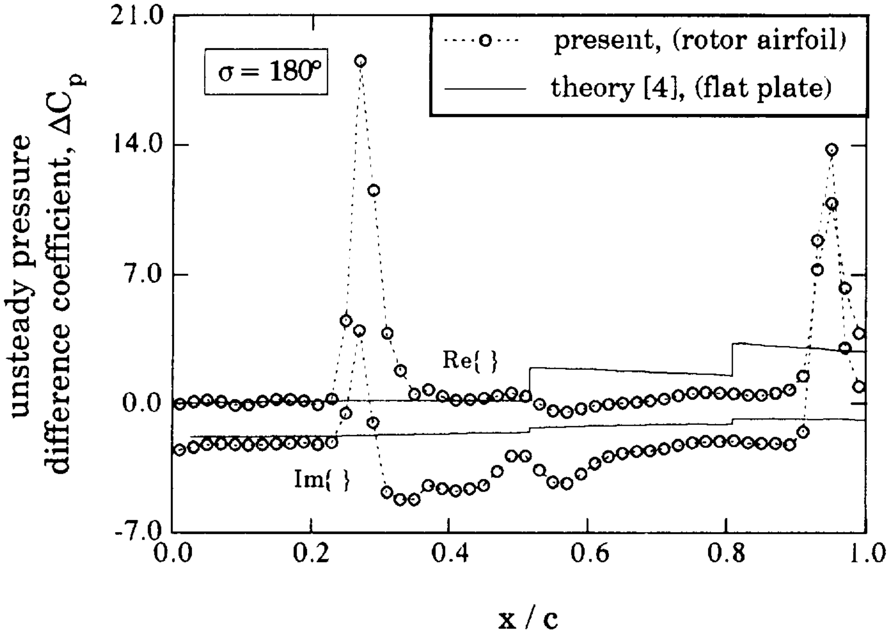

Fig. 18c: Unsteady pressure difference distribution, $\sigma = 180$ deg, $k_b = 1.1$, plunging.

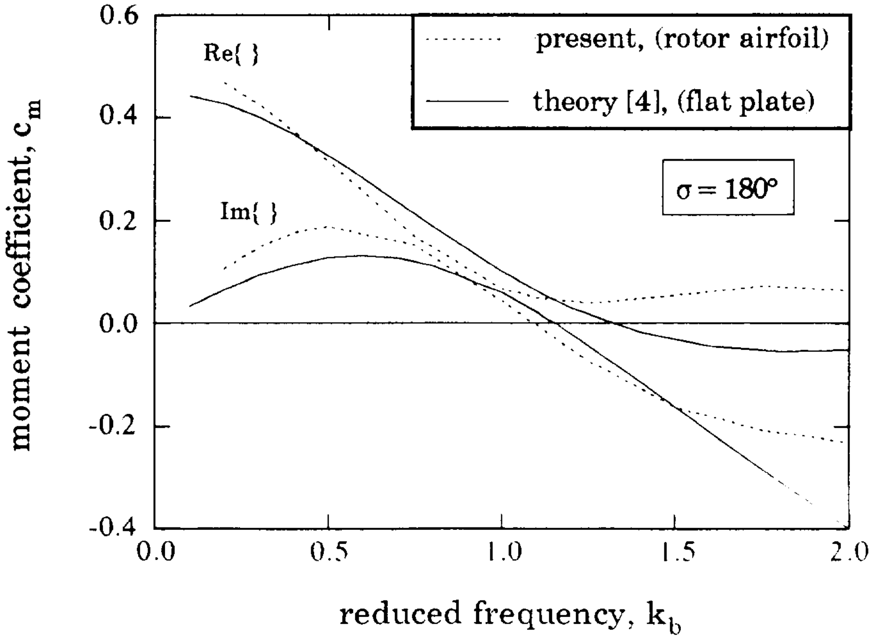

Fig. 19: Comparison of moment coefficient from HO method and linear theory, $\sigma = 180$ deg, pitching, rotor airfoil.

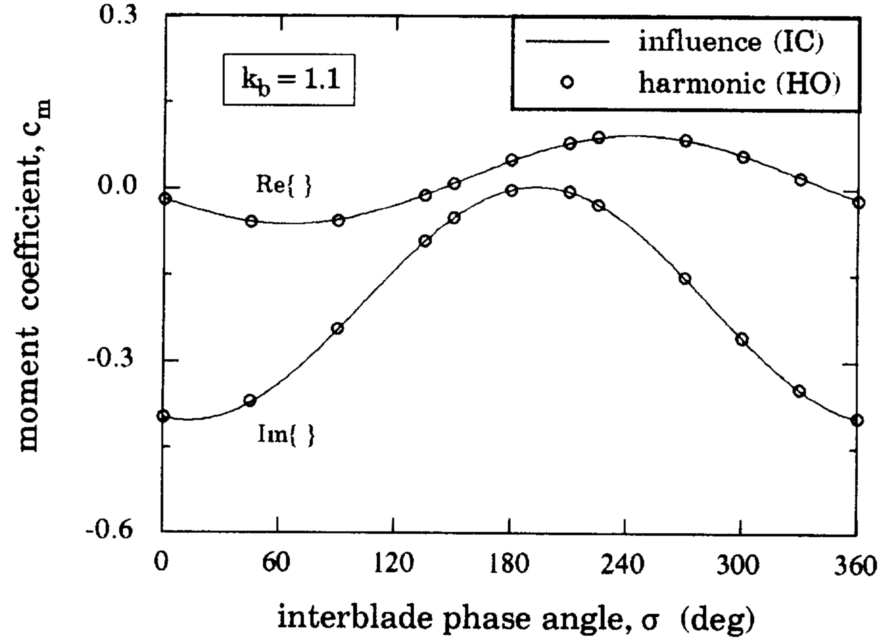

Fig. 20a: Comparison of moment coefficient from HO and IC methods, $k_b = 1.1$, pitching, rotor airfoil.

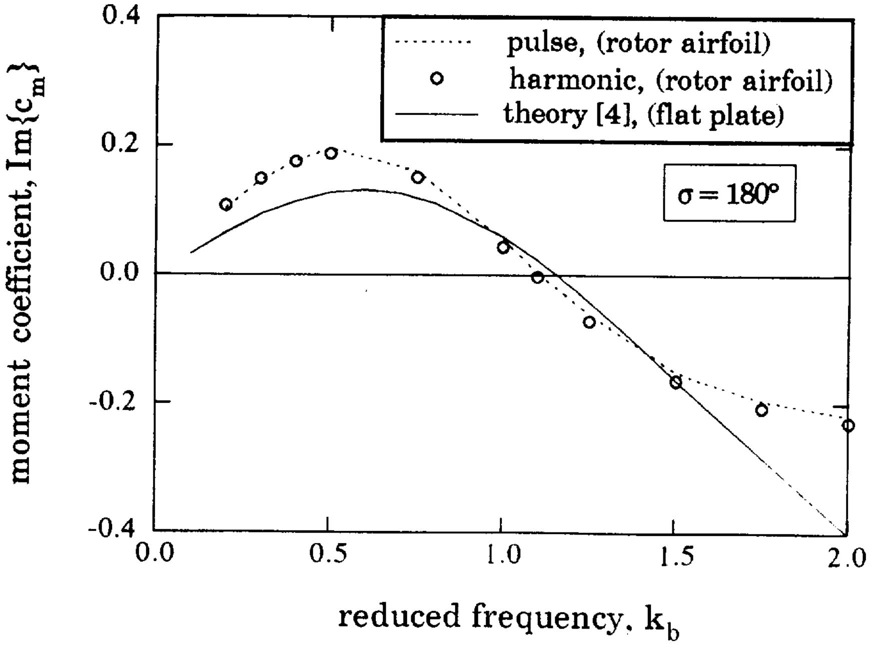

Fig. 20b: Comparison of moment coefficient from HO and PR methods, $\sigma = 180$ deg, pitching, rotor airfoil.

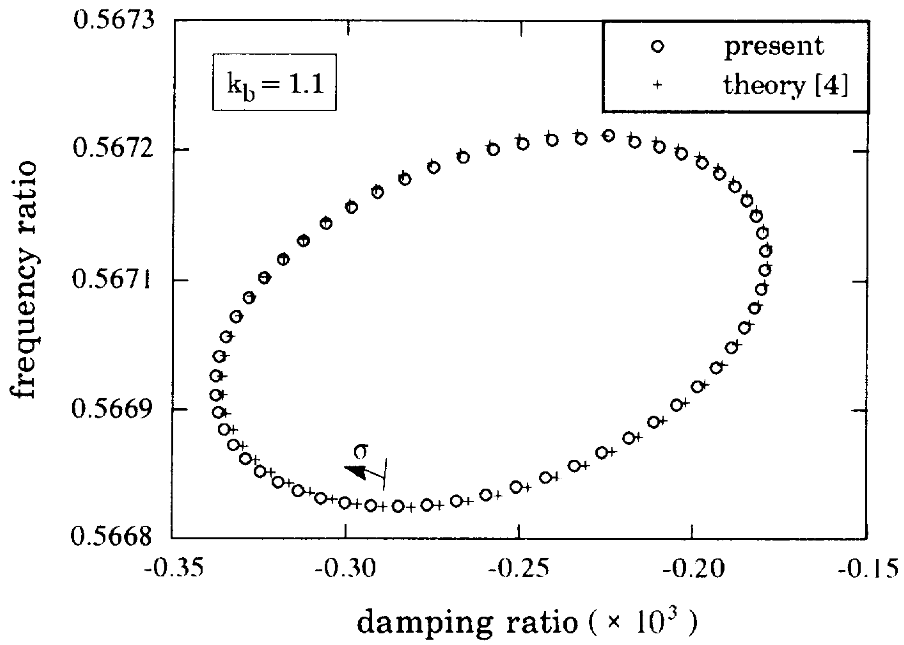

Fig. 21a: Comparison of root locus plot from present analysis and linear theory, $k_b = 1.1$, flat plate cascade, first mode; $\sigma = 0, 6.2, 12.4, \ldots, 173.8, 180, 186.2, 192.4, \ldots,$ and 353.8 deg in the direction indicated by the arrow.

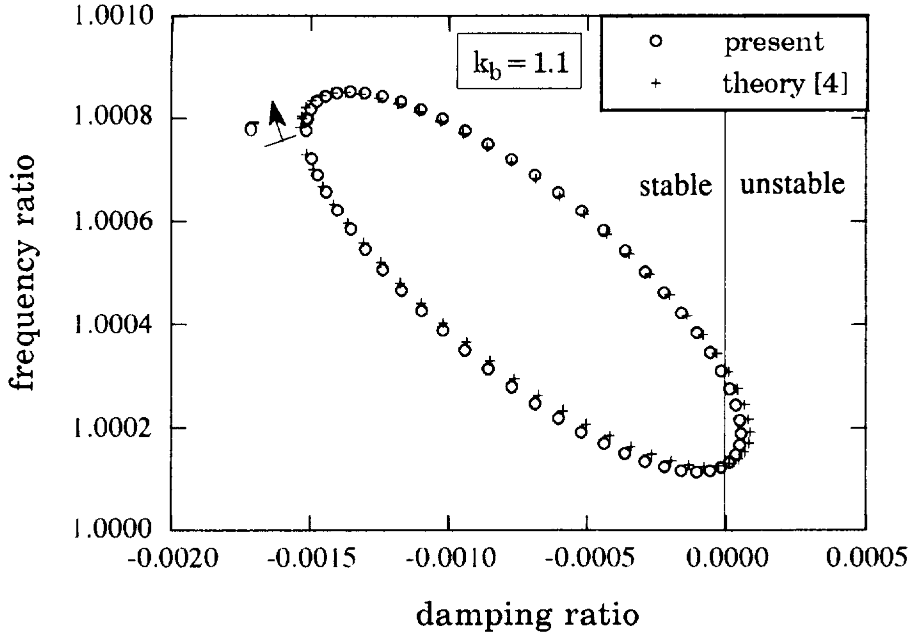

Fig. 21b: Comparison of root locus plot from present analysis and linear theory, $k_b = 1.1$, flat plate cascade, second mode; $\sigma = 0, 6.2, 12.4, \ldots, 173.8, 180, 186.2, 192.4, \ldots,$ and 353.8 deg in the direction indicated by the arrow.

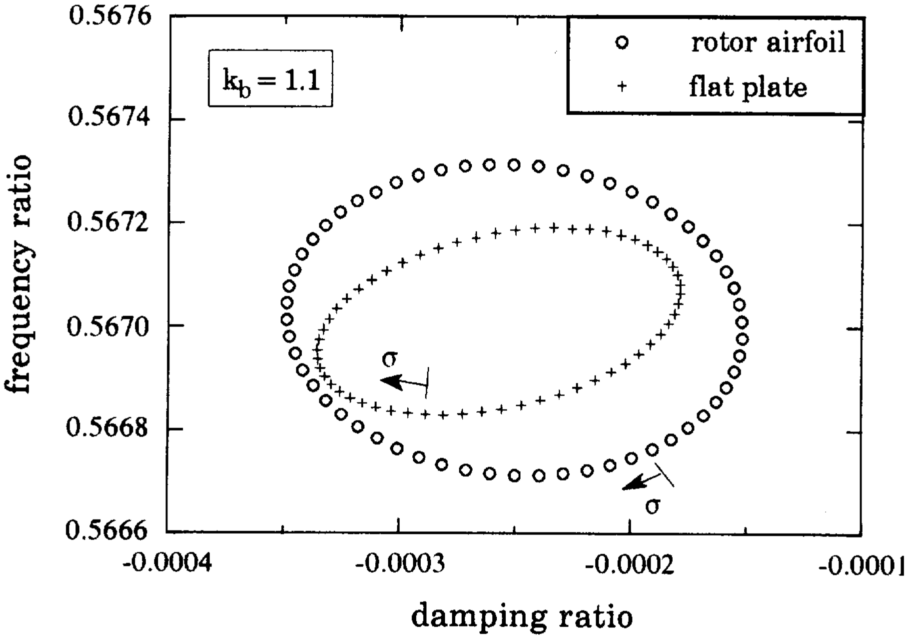

Fig. 22a: Root locus plot from present analysis, $k_b = 1.1$, first mode; σ = 0, 6.2, 12.4, ..., 173.8, 180, 186.2, 192.4, ..., and 353.8 deg in the direction indicated by the arrow.

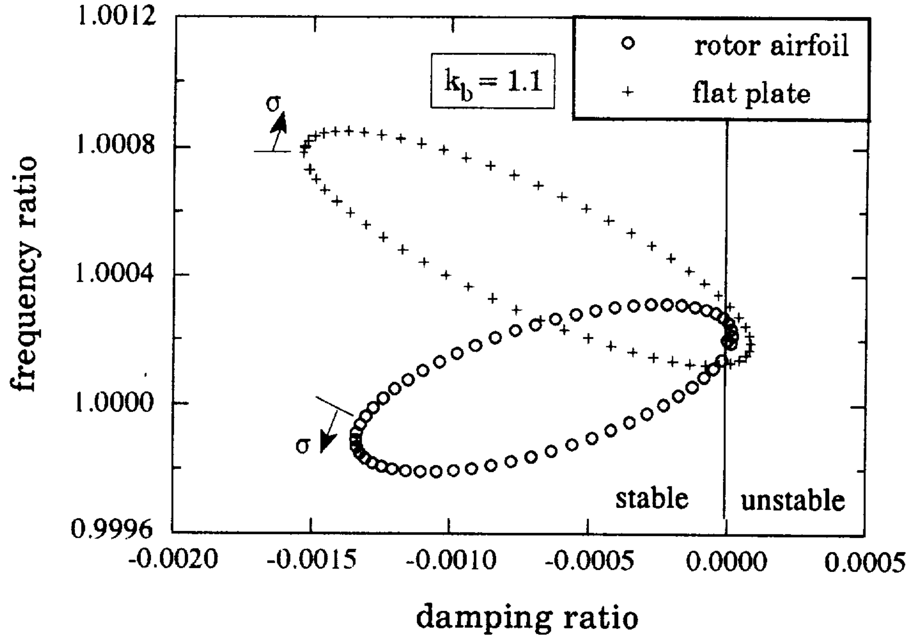

Fig. 22b: Root locus plot from present analysis, $k_b = 1.1$, second mode; σ = 0, 6.2, 12.4, ..., 173.8, 180, 186.2, 192.4, ..., and 353.8 deg in the direction indicated by the arrow.

REPORT DOCUMENTATION PAGE

Form Approved
OMB No. 0704-0188

1. AGENCY USE ONLY *(Leave blank)*

2. REPORT DATE
August 1992

3. REPORT TYPE AND DATES COVERED
Technical Memorandum

4. TITLE AND SUBTITLE
Flutter Analysis of Supersonic Axial Flow Cascades Using a High Resolution Euler Solver
Part 1: Formulation and Validation

5. FUNDING NUMBERS
WU-535-03-10

6. AUTHOR(S)
T.S.R. Reddy, Milind A. Bakhle, Dennis L. Huff, and Timothy W. Swafford

7. PERFORMING ORGANIZATION NAME(S) AND ADDRESS(ES)
National Aeronautics and Space Administration
Lewis Research Center
Cleveland, Ohio 44135-3191

8. PERFORMING ORGANIZATION REPORT NUMBER
E-7229

9. SPONSORING/MONITORING AGENCY NAMES(S) AND ADDRESS(ES)
National Aeronautics and Space Administration
Washington, D.C. 20546-0001

10. SPONSORING/MONITORING AGENCY REPORT NUMBER
NASA TM-105798

11. SUPPLEMENTARY NOTES
T.S.R. Reddy and M.A. Bakhle, University of Toledo, Department of Mechanical Engineering, Toledo, Ohio 43606 and NASA Resident Research Associate at Lewis Research Center. D.L. Huff, NASA Lewis Research Center, Cleveland, Ohio. T.W. Swafford, Mississippi State University, Department of Aerospace Engineering, Mississippi State, Mississippi 39762. Responsible person, George L. Stefko, (216) 433-3920.

12.

Date for general release August 1994
Subject Category 39

2b. DISTRIBUTION CODE

13. ABSTRACT ***(Maximum 200 words)***

This report presents, in two parts, a dynamic aeroelastic stability (flutter) analysis of a cascade of blades in supersonic axial flow. Each blade of the cascade is modeled as a typical section having pitching and plunging degrees of freedom. Aerodynamic forces are obtained from a time accurate, unsteady, two-dimensional cascade solver based on the Euler equations. The solver uses a time marching flux-difference splitting (FDS) scheme. Flutter stability is analyzed in the frequency domain. The unsteady force coefficients required in the analysis are obtained by harmonically oscillating (HO) the blades for a given flow condition, oscillation frequency, and interblade phase angle. The calculated time history of the forces is then Fourier decomposed to give the required unsteady force coefficients. An influence coefficient (IC) method and a pulse response (PR) method are also implemented to reduce the computational time for the calculation of the unsteady force coefficients for any phase angle and oscillation frequency. Part 1, this report, presents these analysis methods, and their validation by comparison with results obtained from linear theory for a selected flat plate cascade geometry. A typical calculation for a rotor airfoil is also included to show the applicability of the present solver for airfoil configurations. The predicted unsteady aerodynamic forces for a selected flat plate cascade geometry, and flow conditions correlated well with those obtained from linear theory for different interblade phase angles and oscillation frequencies. All the three methods of predicting unsteady force coefficients, namely, HO, IC and PR showed good correlation with each other. It was established that only a single calculation with four blade passages is required to calculate the aerodynamic forces for any phase angle for a cascade consisting of any number of blades, for any value of the oscillation frequency. Flutter results, including mistuning effects, for a cascade of stator airfoils are presented in Part 2 of the report.

14. SUBJECT TERMS
Cascades; Supersonic axial flow; Flutter; Euler; Harmonic oscillation; Influence coefficient; Pulse response; Frequency domain

15. NUMBER OF PAGES
56

16. PRICE CODE
A04

17. SECURITY CLASSIFICATION OF REPORT
Unclassified

18. SECURITY CLASSIFICATION OF THIS PAGE
Unclassified

19. SECURITY CLASSIFICATION OF ABSTRACT
Unclassified

20. LIMITATION OF ABSTRACT